

Dissolved and particulate carbon export from a tropical mangrove-dominated riverine system

Raghab Ray^{1b},^{1*} Toshihiro Miyajima,¹ Atsushi Watanabe,^{2,a} Masaya Yoshikai,² Charissa M. Ferrera,³ Iris Orizar,^{3,b} Takashi Nakamura^{1b},² Maria Lourdes San Diego-McGlone,³ Eugene C. Herrera,⁴ Kazuo Nadaoka²

¹Atmosphere and Ocean Research Institute, The University of Tokyo, Tokyo, Japan

²School of Environment and Society, Tokyo Institute of Technology, Tokyo, Japan

³Marine Science Institute, University of the Philippines, Diliman, Philippines

⁴Institute of Civil Engineering, University of the Philippines, Diliman, Philippines

Abstract

Despite being a major component in the mangrove carbon (blue carbon) budget, “outwelling” flux (or export to the sea) has gained little attention relative to other biogeochemical fluxes and reservoir carbon stock estimations. This study aims to estimate lateral exchange fluxes of dissolved and particulate organic carbon (DOC, POC) and dissolved inorganic carbon (DIC) from the watershed through a microtidal mangrove-dominated estuary to the coastal sea in Panay Island, Philippines. Along the estuarine transect, consistent addition of DOC, DIC, and POC at higher salinities were attributed to mangrove organic matter input. Upstream groundwater input (carbonate weathering) and downstream mangrove organic matter decomposition (possibly sulfate reduction) were the main controls on DIC. DOC corresponded to relatively pure mangrove sources in creek water, while POC was a mixture of detrital and algal organic matter. The mangrove system acted as net exporter of carbon to the sea in both dry and wet seasons. From short-term observations, outwelling fluxes of mangrove-derived DOC, DIC, and POC contributed 27–53%, 8–31%, and 42%, respectively, to their estuarine outflow. Unlike other studies, such low percentage for DIC might result from other external nonmangrove input (e.g., watershed carbonate weathering). Overall estuarine carbon flux was dominated by DIC (90–95%) with only minor contribution from DOC. The approach utilized in this study to estimate lateral carbon flux specific to a small mangrove setting can be useful in delineating blue carbon budgets that avoid geographical and methodological biases.

The role of coastal interfaces in the carbon cycle is important both for constraining global carbon budgets and representing significant biogeochemical fluxes to the coastal ocean (Ward et al. 2020). Vegetated coastal interfaces such as mangroves, seagrasses, saltmarshes, and macroalgae (also known as “blue carbon” ecosystems) are particularly important as climate change mitigation options because of their large capacity in removing CO₂ from the atmosphere and storing it as organic carbon (OC) within the biomass and sediment for centuries to millennia (Duarte et al. 2005; Howard et al. 2017). Despite their relatively small global surface area (0.07–0.22%), they sequester approximately 65–370 Tg C annually (including the inner shelf areas) which is equivalent to ~10% of the net residual land sink and 50% of carbon

burial in marine sediments (Donato et al. 2011; Fourqurean et al. 2012; Krause-Jensen and Duarte 2016). A significant fraction of this sequestered carbon escapes degradation and gets exported as dissolved and particulate carbon to the sea (Watanabe et al. 2020), while the rest is buried in the sediments depending on sedimentation rates and extent of OC decomposition rate. The “outwelling hypothesis,” or lateral export of wetland biomass material to the sea, was initially put forward for salt marshes by Odum (1968). However, it was later applied to mangroves where export of plant litter was more dominant than their retention due to extensive tidal action (Lee 1995). With growing interest in resolving the carbon budget, the role of mangrove outwelling is now reframed in the context of climate change mitigation or “blue carbon” (Santos et al. 2021).

Among these vegetated coastal habitats, mangroves are the most efficient carbon sinks in the tropics accounting for ~14% of carbon stored by the global coastal ocean giving them a role as CO₂ sink in the global carbon budget (storage

*Correspondence: raghab.ray@aori.u-tokyo.ac.jp, raghab.ray@gmail.com

Additional Supporting Information may be found in the online version of this article.

of $\sim 15\text{--}20$ Pg C on global area basis; Donato et al. 2011). Lines of evidence have revealed that mangroves can export a significant amount of dissolved organic and inorganic carbon (DOC, DIC) and particulate organic carbon (POC) to the sea (Dittmar et al. 2006; Ray et al. 2020; Reithmaier et al. 2020). Mangrove pore water-derived C flux is equivalent to $\sim 30\%$ of global river inputs (Chen et al. 2018). Mangrove-derived export of DIC is considered the largest sink of atmospheric CO_2 in the mangrove carbon budget, while DOC and POC export are also significant components (Maher et al. 2018). The most updated outwelling or lateral carbon flux estimates have reported highest values for DIC (124 Tg C yr^{-1}), followed by DOC (36 Tg C yr^{-1}), and POC (17 Tg C yr^{-1}) with $\sim 75\%$ of the mineralized carbon contributed solely by the dissolved forms within the mangrove soil, and the rest is due to soil respiration (Alongi 2020). However, the carbon outwelling rate has seldom been assessed, mainly because of the difficulty in measurement (according to bibliographic search, the ratio is roughly 50 : 20 published articles on stock : export in 2009–2020; González et al. 2019 and this study). Except for a recent estimate by Taillardat et al. (2018) on dissolved carbon fractions in Vietnam mangroves, there is data scarcity on carbon outwelling flux estimates from Southeast (SE) Asia where mangroves are most abundant ($\sim 46\%$ of global coverage; Giri et al. 2011). Hence, there is a need to increase the number of carbon flux estimates for the SE Asian region.

Different methods for lateral carbon flux estimates in mangrove-dominated coasts have been reported. These are hydrodynamic modeling and estuarine geometry (Sánchez-Carrillo et al. 2009; Ray et al. 2020), cross-sectional monitoring of creeks (Dittmar and Lara 2001; Ohtsuka et al. 2020), flume constructed across creeks (Romigh et al. 2006; Ray et al. 2018), digital elevation modeling (Sippo et al. 2016; Ray et al. 2020), and mass balance approach (Akhand et al. 2021). Estimates can be highly variable at different spatial scales depending on various factors such as seasonal rainfall (wet vs. dry), mangrove settings (riverine, fringing, or basin), tidal regime (i.e., tidal amplitude, symmetry), and terrestrial connectivity via freshwater inputs (Kristensen et al. 2017; Taillardat et al. 2018; Ray et al. 2020). Generally, interior mangroves less exposed to tidal submergence may behave as carbon sink compared to riverine/estuarine mangroves which are generally carbon exporters due to the high material load transported from upstream water discharge (Taillardat et al. 2018). Mangrove-fringed shallow creek water, either connected or disconnected from riverine sources would be more complex because both marine input during high tide and terrestrial export during low tide could drive carbon source-sink characteristics either way during a diurnal cycle (Robertson and Alongi 1995). The existing carbon outwelling flux estimates are mainly derived from the surface water concentration of DOC, POC, and DIC assuming that surface-driven wind and water currents are the major physical controls for the relatively well-mixed water (e.g., Maher et al. 2013; Ho et al. 2017; Ray

et al. 2020). However, this may not always be correct, especially for the river-dominated mangroves where the occurrence of a halocline could mask bottom water carbon concentrations. Hence, the measurement of both surface and bottom water carbon concentrations helps in evaluating actual carbon flux from the mangrove creeks. Furthermore, most of the existing studies on mangrove carbon outwelling are conducted in mesotidal and macrotidal settings, such as the inner shore of the Atlantic Ocean or Bay of Bengal (tidal height 4–5 m; Ray et al. 2018, 2020), but there are very few studies done in microtidal mangroves, for example the Floridan mangroves (< 1 m; Romigh et al. 2006), and no evidence for the entire SE Asian coast.

In this study, we report baseline estimates of carbon export from a microtidal old-growth mangrove system in the Philippines, where diversity of the trees is high and mangrove cover comprises 1.9% of the global mangrove area (Giri et al. 2011). The spatial and temporal variability of shallow creek water carbon composition was determined, while the source and export fluxes were estimated. Stable isotope ratios of carbon and nitrogen were used to trace sources of terrestrial and aquatic organic matter (Gilbert et al. 2019). Our main objectives are (1) to quantify the spatiotemporal concentrations of DOC, POC, and DIC and their isotope ratio ($\delta^{13}\text{C}$) in various water bodies within the mangrove domain (river, creek, offshore, pore water, groundwater) and (2) to estimate the seasonal carbon outwelling fluxes from the river to the estuary to the coastal sea by performing time series water column sampling at multiple locations and applying hydrodynamic modeling of the tidal creek.

Materials and methods

Study site description

The study was conducted at Katunggan It Ibajay (KII) Ecopark (11.806°N , 122.202°E , Fig. 1), which is located in the municipality of Ibajay in Aklan province of Panay Island, Philippines. The KII Ecopark is home to one of the most diverse mangrove forests in the country. The total land area of KII Ecopark is 0.44 km^2 (Barrientos and Apolonio 2017), boasting a total of 28 true mangrove species or 80% out of the total 35 mangrove species in the Philippines (Primavera et al. 2004). Mangroves in the area are undisturbed and very productive; dominated by a climax forest of large, old *Avicennia rumphiana* and *Avicennia officinalis* (locally known as bungalon or apiapi) surrounded by zones of mixed *Avicennia marina*, *Bruguiera sexangula*, planted *Ceriops tagal* and numerous *Nypa fruticans* (Suwa et al. 2020). *A. rumphiana* and *A. marina* of less than 15-m height dominate at the seaward zone. Notably, at the KII Ecopark is a giant *A. rumphiana* tree (8-m circumference), which is included in the Mangrove Watch's list of oldest and biggest mangroves in the world.

Located within less than 1 km from the Sibuyan Sea with land-facing elevations from 0.4 to 1 m, the study sites are comprised of three connected tidal creeks with shallow depth

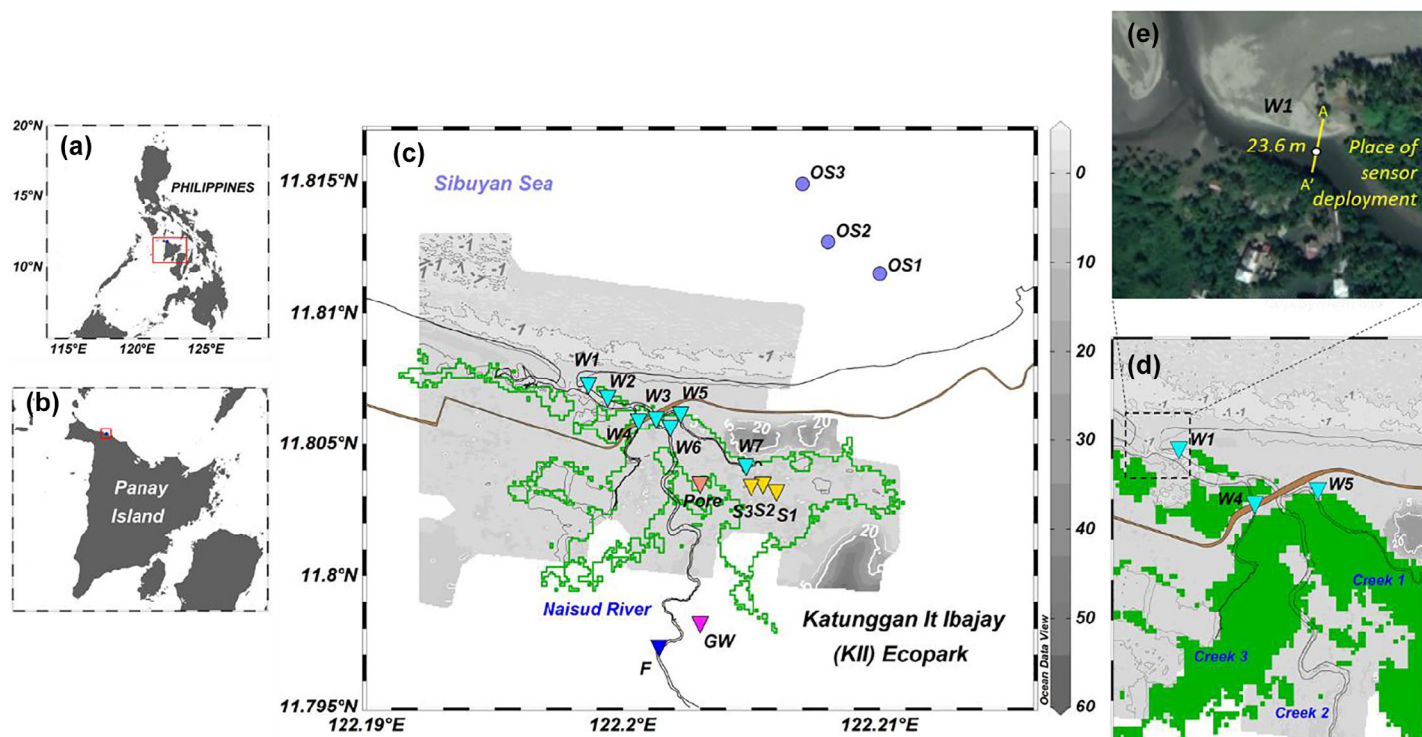


Fig. 1. Map of sampling stations at the KII Ecopark, Panay Island, Philippines (panel **a**, **b**). The mangrove area is delineated by the green contour lines (panel **c**) and shaded in green (panel **d**). It is overlain on digital elevation model data resampled every 5 m. Contour lines for 1-m depth (gray broken lines), MSL (0 m; black lines), and 5-m (thin white lines) and 20-m (bold white contours) elevation are shown. Time series stations W5 and W4 are also shown, as well as the sensor deployment site near W1 close to the river mouth. The brown line represents a public road. The yellow line in panel **e** indicates the transect line of the river cross-sectional measurement. Site abbreviations are as follows: F, fresh water, GW, groundwater; OS series, offshore water; Pore, pore water; S series, swamp water; W series, creek water.

(~1.5 m) and common narrow exit channel to the sea, and an upstream freshwater connection with the Naisud River. Most of the mangrove species are distributed throughout the length of the creeks. This microtidal riverine mangrove has only one entrance for seawater flow; therefore, it is a candidate site for area-based estimates of carbon exchange fluxes between the mangroves and the sea.

The KII Ecopark experiences a clear semidiurnal microtidal cycle (two tidal cycles per day, high tide amplitude < 1.5 m) and is influenced by seawater and river water. The mangrove forest floor is fully inundated during spring tides, but some parts are not flooded during neap tides. The narrow salinity (*S*) range between the inner shore, creek mouth, and inside creek water during high tide ($S \sim 25\text{--}30$) suggests complete tidal flushing from the sea end. There is no pronounced maximum rainy season. There are short dry periods of 1–3 months (December to February or March to May), and the rest of the year represents wet season (monthly rainfall 266 ± 125 mm in 2017–2018; retrieved from JRA-55 Reanalysis, Kobayashi et al. 2015).

Geologically, the north-western peninsula of Panay Island or Buruanga peninsula is an example of Lagdo formation dominated by lithic fragments composed mostly of ultramafic and volcanic rocks (44–86%), with feldspar (6–11%), matrix

components (1–23%), and very few quartz grains (~1–10%) (Gabo et al. 2009). Depending on the mangrove zonation, slightly acidic sediments at KII Ecopark usually contain higher silt than sand and clay (Leбата 2006) with low OC% (mean 1.6%; Barrientos and Apolonio 2017).

Sampling procedure

Two field campaigns were conducted at the KII Ecopark at different seasonal conditions from 06 September 2017 to 09 September 2017 (wet season) and from 23 February 2019 to 02 March 2018 (dry season). Sampling strategies are graphically explained in the Supporting Information (Fig. S1). Surface and bottom water sampling was conducted using a boat along the creek water downstream to offshore water. At each sampling point, location was recorded using a Global Positioning System receiver. Upstream river waters were sampled from the bridge at specific locations. Groundwater samples were collected from a nearby regularly used domestic tube well ($S = 0$) following prescribed guidelines (U.S. Office of Surface Mining Reclamation and Enforcement 21 May 2012; see references therein). Inside the mangrove mudflat, swamp water samples (considered as mixture of groundwater and tidal water) were siphoned from the surface using a 50-mL plastic syringe. As representative of water seeping out of the

mangrove sediments, pore waters were obtained by digging ~ 0.5–1 m of mud and using a tube to siphon the water. Sampling stations were assigned the W series (W1–W7) for creek water, F for river water, OS for offshore water, and S for swamp water. Time series observations were done in W5 for 24 h at 30-min intervals, and on occasional hourly basis at W4 in both surveys (06–07 September 2017 and 26–27 February 2018). It was spring tide during the time series survey in September (max. height 0.75 m) and transition from neap to spring tide in February (max. height 0.66 m). The mean sea level (MSL) at Stas. W5 and W4 was derived by averaging the water depth fluctuations for the entire 24-h monitoring period. The water level (relative to the MSL) was derived by subtracting the MSL from the water depth.

All water samples were collected to determine the dissolved (TA, DIC, DOC, their isotope ratios as $\delta^{13}\text{C-DIC}$, $\delta^{13}\text{C-DOC}$, and Radon-222 [^{222}Rn] isotope) and particulate (total suspended solids [TSS], POC, particulate nitrogen [PN], their isotope ratios as $\delta^{13}\text{C-POC}$, $\delta^{15}\text{N-PN}$, and chlorophyll *a* [Chl *a*] parameters.

In situ water column profiles of temperature ($^{\circ}\text{C}$), salinity, turbidity (Formazine Turbidity Unit, FTU), Chl *a* ($\mu\text{g L}^{-1}$) and dissolved oxygen saturation (DO, %) were acquired at every sampling station using an AAQ-RINKO water quality profiler (JFE-Advantech, Japan) prior to water sampling. Surface and bottom water samples were collected by a Niskin sampler (5 L, General Oceanics) at W and OS, and manually using a bucket from upstream at F, and from the domestic tube well.

In the field, water samples for DOC, $\delta^{13}\text{C-DOC}$, and Chl *a*, were prefiltered through a 200- μm sieve attached to a plastic funnel and collected into polypropylene containers. The DOC and $\delta^{13}\text{C-DOC}$ samples were further filtered through single-use disc filters (ADVANTEC, hydrophilic polytetrafluoroethylene, 0.45 μm pore size) attached to 50-mL glass syringe and collected in amber vials (teflon-lined caps). The DOC and isotopic samples were preserved after addition of 2 M HCl until pH decreased to 2. The TA and DIC samples were collected by overfilling 250-mL borosilicate bottles and adding saturated HgCl_2 solution (200 μL) as preservative. Samples for $\delta^{13}\text{C-DIC}$ (10-mL glass vials with teflon-lined screw caps) were filtered immediately through syringe filters (ADVANTEC, cellulose-acetate membrane, 0.8 μm pore size). Samples for $\delta^{13}\text{C-DIC}$ were preserved with saturated HgCl_2 solution (100 μL) and were capped without air bubbles inside the bottles.

In the laboratory, known volumes of water samples (~ 2 L) were filtered onto preweighed and precombusted (450 $^{\circ}\text{C}$, 3 h) 47-mm glass fiber filters (Whatman GF/F, 0.7 μm pore size, Whatman GE Healthcare Life Sciences, England) for TSS, POC, and PN analysis. Filters for TSS were subsequently oven dried at 105 $^{\circ}\text{C}$ for 1 h repeatedly until constant weight (< 0.5 mg weight change) was achieved. For Chl *a* analysis, at least 100 mL sample was filtered onto precombusted (450 $^{\circ}\text{C}$, 3 h) 25-mm glass fiber filter (0.7 μm pore size) after which the filters were immersed in 6 mL *N,N*-dimethylformamide. Both filters of POC/PN (their isotopes) and Chl *a* were kept in the dark at -20 $^{\circ}\text{C}$ until

measurement. All samples of dissolved parameters except for TA, DIC, and $\delta^{13}\text{C-DIC}$ were kept frozen until their analyses.

Concentrations of the ^{222}Rn radioisotope were measured in the water using the showerhead equilibration technique (Blanco et al. 2011) during the dry season only. Briefly, water samples collected in 250-mL glass bottles were allowed to overflow and brought immediately to the laboratory for analysis using RAD7 (a radon-in-air monitor) and RAD-H₂O systems (DurrIDGE Company).

Chemical analysis

DOC concentration was determined by high-temperature combustion oxidation (Shimadzu TOC-L Analyzer). Small volumes (100 μL) of the filtered acidified water samples were sparged with oxygen to remove inorganic carbon. Nonpurgeable OC compounds were combusted at 650 $^{\circ}\text{C}$ and converted to CO_2 , which was detected by a nondispersive infrared sensor. The instrument was calibrated by a series of aqueous solutions of potassium hydrogen phthalate and washed several times with Milli-Q water to minimize the coefficient of variation. The reproducibility of DOC measurements was usually < 2%. The bulk measurement of DOC stable isotope ratio ($\delta^{13}\text{C-DOC}$) was carried out by wet chemical oxidation using a high-performance liquid chromatography (LC) system coupled to a Delta⁺ XP isotope-ratio mass spectrometer (IRMS) through a LC IsoLink interface (Thermo Fisher Scientific). The $\delta^{13}\text{C-DOC}$ values were reported relative to the Pee Dee Belemnite standard with an overall uncertainty of $\pm 0.1\%$. Details of the LC-IRMS system and modifications are given elsewhere (Scheibe et al. 2012).

Total alkalinity (TA) of seawater samples ($S > 20$) was measured by potentiometric titration with 0.1 N HCl using an automated closed cell Total Alkalinity Titrator (Kimoto, ATT-05) (Kurihara et al. 2021). The accuracy and the precision of measurements were verified using certified reference materials distributed by A. Dickson (Scripps Institution of Oceanography). DIC and CO_2 concentrations (hereafter expressed as $[\text{CO}_2^*]$) were computed from TA and pH using the software CO2SYS.EXE (Lewis and Wallace 1998). DIC of freshwater and brackish waters ($S < 20$) was measured using the Shimadzu TOC-L Analyzer (IC mode) calibrated against 2 and 5 mM NaHCO_3 solutions. The reproducibility for DIC was $\pm 4 \mu\text{mol kg}^{-1}$. The $\delta^{13}\text{C-DIC}$ was determined by the headspace-equilibration method. A 0.5–2.0 mL portion (depending on DIC concentration) of HgCl_2 -amended water sample was added by a microsyringe to a 10-mL screwcapped tube with rubber septum containing 20 μL of phosphoric acid and was purged with pure helium in advance. The headspace gas of the tube was equilibrated overnight, and then introduced to Gasbench-IRMS (Thermo Fisher Scientific, DELTA V) using an autosampler to determine the $\delta^{13}\text{C}$ of CO_2 . Standards such as NBS19 (TS-Limestone) and LSVEC (Li-carbonate) were used as International Standards while SPK was used as working standard

during calibration. The analytical error was within 0.2‰ for $\delta^{13}\text{C}$ -DIC.

The Chl *a* concentration in *N,N*-dimethylformamide extract was measured fluorometrically (Turner Designs, 10AU) with photometric precision < 0.5% at 1 absorbance unit. POC and $\delta^{13}\text{C}$ -POC were determined by an Elemental Analyzer-IRMS (FLASH 2000/Conflo IV/DELTA V Advantage, Thermo Fisher Scientific) for the 47-mm filter samples after pre-treatment with fuming HCl (Sato et al. 2006). The measured isotope ratios were represented using the conventional δ -notation ($\delta^{13}\text{C}$ and $\delta^{15}\text{N}$) with Vienna Pee Dee Belemnite and atmospheric N_2 as the reference materials. Three to five standard materials of different $\delta^{13}\text{C}$ and $\delta^{15}\text{N}$ were used for daily calibration (SI Science Ltd and Iso-Analytical Ltd). The instrument analytical precision was normally within $\pm 1\%$ for the OC and total nitrogen concentrations, and $\pm 0.1\%$ for $\delta^{13}\text{C}$ and $\delta^{15}\text{N}$.

Mixing model calculations to derive residual carbon

To quantify the “addition” or “removal” of DOC/DIC/POC by biogeochemical processes at various salinities in the study sites, a simple two-component mixing model (modified from Carpenter et al. 1975) was used.

$$C_{\text{CM}} = \frac{S \times C_{\text{M}} + (S_{\text{M}} - S)C_{\text{R}}}{S_{\text{M}}} \quad (1)$$

The C_{CM} denotes concentration derived by conservative mixing. The S and S_{M} represent observed and marine end-member salinity (here as ~ 32), respectively, while C_{R} and C_{M} are the riverine and marine end-member concentrations, respectively. Positive/negative differences of actual concentration from C_{CM} in Eq. 1 indicate sources/sinks or the transformation of C within the mangrove waterways.

Residual carbon concentration either “added” or “subtracted” (ΔC_{CMM}) at any given salinity during the transport can be estimated by considering the difference between observed (C_{obs}) and C_{CM} of DOC, DIC, and POC. This value, according to Alling et al. (2012), can be expressed as follows:

$$\Delta C_{\text{CMM}} = C_{\text{obs}} - C_{\text{CM}} \quad (2)$$

Stable isotope signatures were included into this mass-balance equation to evaluate the sources/sinks of carbon following the general conservative mixing equation adapted from Mook and Tan (1991):

$$\delta^{13}\text{C}_{\text{CM}} = \frac{(C_{\text{M}}\delta^{13}\text{C}_{\text{M}} - C_{\text{R}}\delta^{13}\text{C}_{\text{R}})S + C_{\text{R}}S_{\text{M}}\delta^{13}\text{C}_{\text{R}}}{(C_{\text{M}} - C_{\text{R}})S + C_{\text{R}}S_{\text{M}}} \quad (3)$$

Here, $\delta^{13}\text{C}_{\text{CM}}$ is the carbon isotope ratio derived from conservative mixing, $\delta^{13}\text{C}_{\text{R}}$ and $\delta^{13}\text{C}_{\text{M}}$ are the riverine and marine end-member isotope ratios of the different carbon fractions (DOC, POC, and DIC), respectively.

Because positive ΔC includes “added” C from mangrove and other sources such as algal excretion and carbonate dissolution, we estimated the isotopic composition of the residual C component ($\delta^{13}\text{C}_{\text{a}}$) by denoting “added” C here, thus following the equation below (Ray et al. 2018):

$$\delta^{13}\text{C}_{\text{a}} = \frac{(\delta^{13}\text{C}_{\text{obs}}C_{\text{obs}}) - (\delta^{13}\text{C}_{\text{CM}}C_{\text{CM}})}{\Delta C_{\text{CMM}}} \quad (4)$$

As stated in Eq. 2, the model value of ΔC_{CMM} (Model 1) would represent internally produced carbon within the estuarine transect. However, for verification of this C whether being same as or different from mangrove origin (C_{mangrove} , model 2), another simple mass balance equation was applied that was modeled by Miyajima et al. (2009) originally for quantifying mangrove-derived DIC in SE Asian mangrove estuaries.

$$C_{\text{obs}}\delta^{13}\text{C}_{\text{obs}} = C_{\text{CM}}\delta^{13}\text{C}_{\text{CM}} + C_{\text{mangrove}}\delta^{13}\text{C}_{\text{mangrove}} \quad (5)$$

Here, C_{mangrove} is mangrove-derived concentration, while $\delta^{13}\text{C}_{\text{mangrove}}$ denotes the $\delta^{13}\text{C}$ value of *Avicennia* plant tissue (-28% ; Ray et al. 2018). This equation assumes that non-conservative changes of DOC, DIC, POC, and their isotope ratios are influenced primarily by the input of their mangrove-derived fractions, and that no other process significantly affects the C balance except mixing.

Hydrodynamic measurement to calculate the carbon exchange rate

Sensors for long-term monitoring of hydrodynamics were deployed at the river mouth (11.8047°N, 122.2094°E; Fig. 1e) from September 2017 to June 2018 to cover both wet and dry seasons. The location of sensor deployment in the river cross-section where flow velocity is heterogeneous was slightly different during the wet and dry season measurements. It was shallower during the dry season than the wet season, hence flux comparison was done separately for the wet and dry seasons. After sensor deployment, river cross-sectional topography at the river mouth was measured and river topography was corrected to MSL (see Supporting Information for more details on the measurement and Fig. S2).

Water exchange rate (Q_{w}) between the estuary and the sea was estimated by multiplying the measured flow velocity and the river cross-sectional area at 30-min interval for the entire 24-h sampling period in both wet and dry seasons. Based on comparisons between the estimated (from the sensors) and measured (from the multipoint velocity measurement) water flux values, the values for the dry season were calibrated against the measured data for the actual river water flux, while values for the wet season were used as the actual values without calibration (see Supporting Information Figs. S3, S4). The estuarine C exchange flux (mol h^{-1}) was then estimated on an hourly basis by multiplying the observed C concentration (C_{obs}) with Q_{w} . Similarly, mangrove-derived carbon exchanges

were calculated by multiplying ΔC_{CMM} of the respective DOC, POC, and DIC in Eq. 2 with Q_w . Both C_{obs} and ΔC_{CMM} are averages of their surface and bottom water concentrations at W5 and W4. Positive exchange fluxes indicate C export from land to sea (outwelling), while negative fluxes denote import from sea to land (inwelling). Carbon flux rate was further estimated at the ground area basis by dividing the calculated carbon exchange rate (both estuarine- and mangrove-derived) by the tidal inundation area. The inundation area during the highest tide (~ 1.2 m above MSL) was estimated as 0.39 km^2 from a LiDAR-derived digital elevation model for the area (a product of Phil-LiDAR 1 Program; Fig. 1c), and this value was used for the area-weighted flux calculation.

Watershed models to calculate riverine carbon discharge

To quantify the C influx from the upstream river discharge to KII Ecopark where the freshwater end-member water samples were collected, and to determine its contribution to the C export rate to the ocean, the simulated river discharge was used (Hernandez et al. pers. comm.). The simulation for Naisud River from 1981 to 2013 was based on a watershed model Soil and Water Assessment Tool (SWAT; Tan et al. 2019). The river discharge values in February and September were extracted from SWAT and averaged for the whole simulation period as representative values of the dry and wet season, respectively (Supporting Information Fig. S5). Finally, the riverine carbon export (mol h^{-1}) was estimated by multiplying the mean observed carbon concentration at the river site F (C_R) with Q_R for both dry and wet seasons.

Statistical analysis

The differences in parameters among water sources during the dry season (creek, groundwater, offshore, swamp) were compared using ANOVA. Data transformation was performed on parameters where heteroscedasticity (Levene's test, "car" package) and/or non-normal distribution (Shapiro-Wilk test, "stats" package) were detected. Pairwise comparison using Tukey's honestly significant difference was used whenever ANOVA results indicated significant influence on main effects (p -value < 0.05). The effect of seasons (dry and wet season) on the sampling stations was determined using two-factor ANOVA. Only the stations that have observations for both dry and wet season were included in this analysis. All statistical analysis was performed using R software (Version 4.0.3) and following Wickham et al. (2020).

Results

Spatio-temporal variabilities of observed parameters

The ranges and trends of all measured parameters varied between the two surveys (Fig. 2a–h, Table 1). There were significant variations of most of the measured physico-chemical and carbon parameters among different water sources (creek, swamp, groundwater, offshore) present within the short sampling transect during the dry season

($p < 0.05$, Supporting Information Table S1). Offshore sites had higher salinity, pH, and DO than the estuarine sites, whereas TSS, TA, and dissolved carbon parameters were higher in creek water and freshwater sites. Significant seasonality was observed for salinity, pH, $[\text{CO}_2^*]$, and $\delta^{13}\text{C}$ -DIC ($p < 0.05$).

Surface water DOC varied widely from 40 to $1083 \mu\text{mol L}^{-1}$ ($n = 43$, Fig. 2a), with maximum concentration observed in the pore water (Table 1). In the dry season, $\delta^{13}\text{C}$ -DOC was generally stable in the surface water with minimum values in swamp water ($-27.6\text{‰} \pm 1.2\text{‰}$, $n = 23$, Fig. 2b). Surface water DIC showed nonconservative behavior with values ranging from 1899 to $4873 \mu\text{mol L}^{-1}$ ($n = 33$, Fig. 2c). There were significant seasonal differences in $\delta^{13}\text{C}$ -DIC ranging from 0.5‰ to -15.8‰ ($n = 41$, $p = 0.01$, Fig. 2d, Supporting Information Table S1). TA decreased with salinity, similar to DIC for salinity > 20 (2183 – $4772 \mu\text{mol L}^{-1}$, $n = 13$, Fig. 2e). Mean surface water ^{222}Rn concentration significantly increased from 73 Bq m^{-3} in offshore waters to 1925 Bq m^{-3} in pore waters ($n = 33$, $p = 0.003$, Fig. 2f). Mean POC concentrations increased from $17.4 \mu\text{mol L}^{-1}$ in the offshore surface water to a maximum of around $65 \mu\text{mol L}^{-1}$ (3.5%) in the creek and swamp waters ($n = 40$, Fig. 2g). The mean values of POC/TSS % (w/w) were higher in the offshore water (5.5%) than the creek water (3.5%, data not shown). A wide range in $\delta^{13}\text{C}$ -POC was observed from offshore to creek waters (-22‰ to -28‰ , $n = 40$, Fig. 2h).

Variation in water characteristics over tidal cycle

Time series observations revealed a dynamic tidal creek where seawater flowed into creeks during high tide (evidenced by negative values of water flow) and river water flowed out to sea during low tide (Fig. 3a–d). Surface water salinity increased from 3 to 32 during low to high tide transition in the dry season (except for few drops between 19 : 00 and 21 : 00); however, salinity variation was less in the wet season (24–33). From the multiparameter profiling (AAQ), the presence of salinity stratification was observed at W5 and W4, but such trend was less prominent in the wet season (refer to Supporting Information Fig. S6). The AAQ profiling showed higher DO% during the rising tide, and higher Chl *a* during the low tide.

The tidal pattern of DOC concentration was consistent with site and season ($n = 57$, Fig. 3e,f), where maximum values were seen during the onset of low tide (dry: $264 \mu\text{mol L}^{-1}$, wet: $231 \mu\text{mol L}^{-1}$) and minimum values during the high tide periods (dry: $91 \mu\text{mol L}^{-1}$, wet: $65 \mu\text{mol L}^{-1}$). During the daytime (10 : 00 to 17 : 00), bottom water DOC concentration was always higher than the surface value in the dry season, but this trend became opposite at nighttime (23 : 00 to 03 : 00). In contrast, bottom DOC was always lower than the surface water DOC during the wet season. The $\delta^{13}\text{C}$ -DOC displayed a general inverse tidal trend in the dry season, ranging from -25.8‰ to -29.8‰ in the surface water (min.

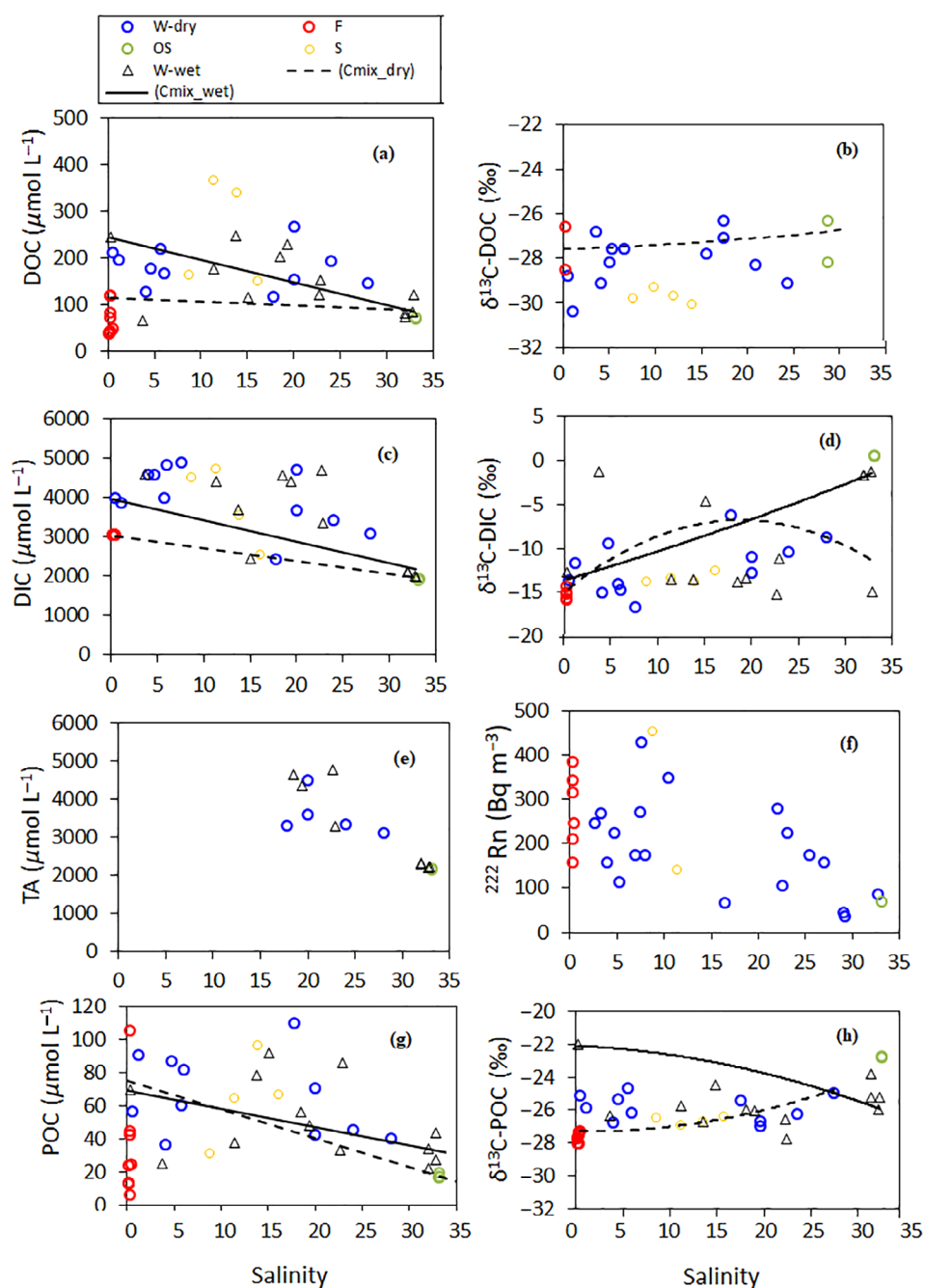


Fig. 2. Scatter plot of carbon and isotope ratio with different salinities in the dry and wet season. Solid and dashed lines represent carbon conservative mixing lines (C_{mix}) in the wet and dry season, respectively.

-30.2‰ at $S = 5$, max. -25.8‰ at $S = 30$, $n = 18$, Fig. 3q). Like DOC, the tidal pattern of DIC was maximum in low tide and minimum in high tide (ranging from 1942 to 4873 $\mu\text{mol L}^{-1}$, $n = 57$, Fig. 3g,h). TA for samples with salinity > 20 mirrored the DIC trend (e.g., dry: 2198–3848 $\mu\text{mol L}^{-1}$). Clear trends during tidal cycles were observed for $[\text{CO}_2^*]$ for both seasons showing consistently higher concentrations during low tide than at high tide (dry: 13–240 $\mu\text{mol L}^{-1}$, wet: 14–205 $\mu\text{mol L}^{-1}$, $n = 44$; Fig. 3i,j). Generally, an increasing

trend of $[\text{CO}_2^*]$ was observed during the night in both seasons (especially during the wet season). Sharp depletions and enrichment in $\delta^{13}\text{C-DIC}$ were observed during the low tide and high tide periods, respectively, for both seasons (min. -14.0‰ , max. $0-0.43\text{‰}$, $n = 57$, Fig. 3m,n). The surface water ^{222}Rn showed clear tidal pattern in the dry season with maximum and minimum values observed for the low and high tide periods, respectively (max. 427 Bq m^{-3} at $S = 8$, min. 35 Bq m^{-3} at $S = 29$, $n = 19$; Fig. 3r).

Table 1. Spatiotemporal water quality parameters, carbon concentrations, and isotope ratios, and natural tracer (^{222}Rn).

Season water sources (station no.)	Salinity	DO %	pH	TSS (mg L^{-1})	Chl <i>a</i> ($\mu\text{g L}^{-1}$)	DOC ($\mu\text{mol L}^{-1}$)	POC ($\mu\text{mol L}^{-1}$)	TA ($\mu\text{mol L}^{-1}$)	DIC ($\mu\text{mol L}^{-1}$)	$[\text{CO}_2]$ ($\mu\text{mol L}^{-1}$)	$\delta^{13}\text{C-DOC}$ (‰)	$\delta^{13}\text{C-POC}$ (‰)	$\delta^{13}\text{C-DIC}$ (‰)	^{222}Rn (Bq m^{-3})
<i>Wet season</i>														
Creek water (W1-W7)	29.5 ± 3	82 ± 24	7.74 ± 0.25	20 ± 12.6	2.6 ± 1.9	147 ± 59	50.6 ± 26.3	3040 ± 836	3150 ± 984	121 ± 91	ND	-25.6 ± 1.1	-7.8 ± 5.4	ND
River water (F)	0.25	76	7.85	4.7	3.5	243	69.5	ND	3980	ND	ND	-22.0	-12.6	ND
<i>Dry season</i>														
Creek water (W1-W7)	14.3 ± 9.8	69 ± 25	7.45 ± 0.15	10.1 ± 8	3.2 ± 1.8	171 ± 42	49 ± 17	3198 ± 616	3730 ± 876	103 ± 74	-28.1 ± 1.1	-25.6 ± 1.0	-11.5 ± 3.8	193.7 ± 105
River water (F)	0.27 ± 0.01	79 ± 7	7.72 ± 0.12	5.9 ± 4.3	3.9 ± 2.6	106 ± 14	51 ± 26	ND	3042	ND	-27.3 ± 0.9	-27.7 ± 0.4	-15 ± 0.44	275 ± 85
Offshore water (OS1-OS3)	33.1 ± 0.05	110 ± 2	8.00 ± 0.01	3.7 ± 4.2	5.3 ± 1.9	72 ± 2	17 ± 1.5	2160 ± 9.5	1907 ± 7	12 ± 0.4	-26.8 ± 1.2	-22.5 ± 0.5	0.54 ± 0.01	87.3 ± 25
Swamp water (S1-S3)	12.5 ± 3.1	52 ± 17	7.22 ± 0.18	10.8 ± 4.3	3.3 ± 0.8	255 ± 113	64 ± 33	ND	3815 ± 1009	ND	-29.7 ± 0.3	-26.6 ± 0.2	-13.4 ± 0.6	296 ± 222
Pore water (Pore)	36	ND	ND	ND	ND	1083 ± 472	ND	6265 ± 408	6629 ± 620	340 ± 203	ND	ND	-16.8 ± 0.14	1925 ± 832
Ground water (GW)	0.27	ND	7.61	1.2	ND	350	6.03	ND	ND	ND	ND	-27.5	-15.6	1290 ± 705

ND, not determined.

POC concentration increased with decreasing tide more prominently during the wet season ($65.50 \mu\text{mol L}^{-1}$ at 17:40, max. low tide; $28 \mu\text{mol L}^{-1}$ at 11:50, max. high tide) than the dry season ($50.34 \mu\text{mol L}^{-1}$ at 10:00, max low tide; $6.50 \mu\text{mol L}^{-1}$ at 17:00, mid high tide, Fig. 3k,l). Bottom water POC concentrations were slightly higher than the surface waters for both time series surveys. Minimum and maximum values for the $\delta^{13}\text{C-POC}$ were measured at low and high salinities, respectively (dry: -27.2‰ to -26.8‰ at $S = 3-5$, and -21.2‰ at $S = 27$, Fig. 3o,p). Average $\delta^{13}\text{C-POC}$ values in the bottom water were more negative than the surface water (-26.8‰ vs. -21.2‰) during the dry season. The POC:Chl-*a* ratio ($\mu\text{g}/\mu\text{g}$; a proxy for the contribution of live biomass to the POC pool) did not show clear tidal variation except for some high values during the low tide ($600-1400 \mu\text{g}/\mu\text{g}$). Low POC:TSS (%) ratios were generally observed during the high tides in both seasons (1.4% in dry, 0.36% in wet). The [POC:PN] atomic ratios were tidally variable and did not differ with seasons (dry: 4-15; wet: 5.5-11) (for all POC:PN data, refer to Supporting Information Fig. S7). TSS in the surface waters varied from ~ 3 to 15mg L^{-1} during the low to high tide transition in the dry season, which was reversed in the wet season (from 48 to 5.8mg L^{-1} , data not shown).

Carbon exchange flux between the mangrove and coastal ocean

Cross-sectional water depths at the hydrodynamic monitoring points of the riverbed varied from 0.12 to 1.4 m (Fig. 2a). The slope-extrapolated width of the river mouth was 23.6 m (Fig. 1e). Hourly water exchange rates (Q_w) were different between the seasons, ranging from -14.70 to $11.62 \text{m}^3 \text{s}^{-1}$ (median 0.78) during the wet season and -4.40 to $5.44 \text{m}^3 \text{s}^{-1}$ (median 0.84) during the dry season. From SWAT modeling, the estimated mean values of the river discharge (Q_R) were 0.53 ± 0.19 and $0.98 \pm 0.79 \text{m}^3 \text{s}^{-1}$ for February 2018 and September 2017, respectively.

The end-members used for model calculations as well as model values are given in Table 2. Except for the significant seasonal differences in the river end-member of DOC ($p < 0.05$, paired *t*-test), other end-member concentrations (C_R and C_M) did not change seasonally, in line with the observed and conservative concentration and stable isotope ratios of DOC, DIC, and POC. Best agreement of results between Model 1 and Model 2 for DIC ($r^2 = 0.94$), DOC ($r^2 = 0.98$), and POC ($r^2 = 0.99$) in the dry season confirms either fraction of carbon (say as ΔC_{CMM} and C_{mangrove} , commonly expressed as ΔC in Fig. 4) can be used in determining the daily exchange fluxes of “internally produced” carbon with the adjacent sea. Except for the negative ΔPOC in the dry season when both models produced positive values for ΔDOC , ΔDIC , and ΔPOC (only wet season), seasonal differences were significant for ΔDIC and ΔPOC ($p < 0.05$, paired *t*-test).

DIC made the largest contribution to the hourly estuarine carbon exchange fluxes between the creek mouth and the sea

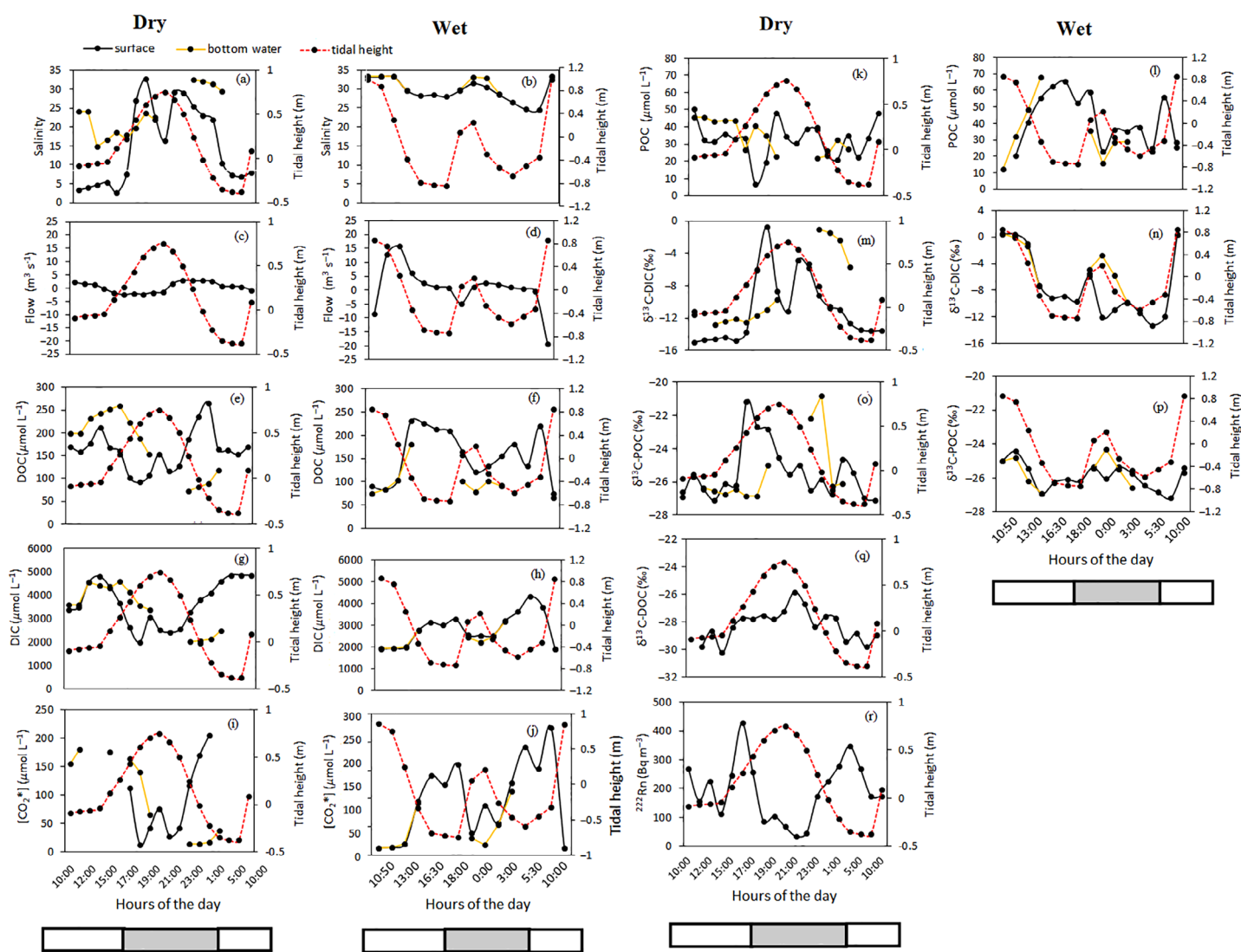


Fig. 3. Seasonal time series observations of carbon and other parameters in the surface and bottom waters at the tidal creek. White and gray bars in the bottom represent day and night time, respectively.

followed by DOC and POC (Fig. 5a–d). The largest export of DIC was observed during the ebb tide in both seasons. Higher fluxes of DOC and POC were observed at the onset of low tide or receding tide. Fluxes of mangrove-derived DIC, DOC, and POC (ΔC) were lower than their daily estuarine fluxes but followed a similar trend. Downstream riverine export (mol h^{-1}) of surface water DOC, DIC, and POC to the adjacent coastal waters of Sibuyan Sea was calculated to be 0.85 ± 0.68 , 14 ± 11 , and $0.24 \pm 0.19 \times 10^3 \text{ mol h}^{-1}$ in the wet season, respectively, and 0.22 ± 0.08 , 5.75 ± 2.14 , and $0.14 \pm 0.05 \times 10^3 \text{ mol h}^{-1}$ in the dry season, respectively (Fig. 6). On an hourly basis, outwelling fluxes of both mangrove- and estuarine-derived carbon exceeded their inwelling fluxes (except for mangrove-POC in the dry season, Fig. 6). Area-weighted estuarine and mangrove-derived fluxes of DOC, DIC, and POC per inundated surface area of mangrove forest (i.e., 0.39 km^2) were estimated to be 16.5 ± 1.7 ,

361 ± 185 , and $4.5 \pm 3.8 \text{ mmol m}^{-2} \text{ d}^{-1}$, and 17.2 ± 6.9 , 140 ± 32 , and $-5.2 \pm 4 \text{ mmol m}^{-2} \text{ d}^{-1}$, respectively.

Discussion

Sources and transport of organic matter

Dissolved organic carbon

The overall DOC in creek waters was lower than reported values for other mangrove-dominated waters (see comparative Table S2 in the Supporting Information) probably due to the short residence time of water (only few tidal cycles) rather than due to differences in DOC formation and decomposition rates. There were 10 times more DOC in pore water and 2 times higher DOC in swamp water compared to waters in creeks. This may be the result of greater organic acids such as humic and fulvic acids leaching from dead roots, litter, and other biogenic

Table 2. Summary of results from end-member mixing models (Eqs. 2–5). Units of concentrations (as C_R , C_M , C_{obs} , C_{CM} , ΔC_{CMM} , $C_{mangrove}$) are as follows: DIC = mmol L⁻¹, DOC, and POC = $\mu\text{mol L}^{-1}$; all isotope results of C are given in ‰. Slopes and offsets (intercepts) derived from fitted linear regression lines are given in the parentheses against C_{CM} . The following forms of carbon C_R , C_M , C_{obs} , C_{CM} , ΔC_{CMM} , C_a , and $C_{mangrove}$ indicate riverine, marine, observed, conservative, residual, added, and mangrove-derived, respectively.

Carbon	C_R	C_M	$\delta^{13}C_R$	$\delta^{13}C_M$	C_{obs}	$\delta^{13}C_{obs}$	C_{CM}	$\delta^{13}C_{CM}$	ΔC_{CMM}	$\delta^{13}C_a$	$C_{mangrove}$
<i>Wet season</i>											
DOC	243	84	-27.6	ND	160 ± 57	ND	104 ± 14 (-4.8, 246)	ND	55 ± 59	ND	ND
DIC	3.98	2.14	-12.7	-1.24	3.04 ± 0.88	-7.5 ± 5.2	2.41 ± 0.2 (-0.05, 4.1)	-3.4 ± 1.6	0.78 ± 0.8	-26.8 ± 49	0.40 ± 0.25
POC	69.4	33.1	-22.0	-25.6	42 ± 16	-26 ± 0.7	38 ± 3.3 (-1.1, 69.5)	-26.3 ± 0.7	4.5 ± 15	-25 ± 5	4.1 ± 14
<i>Dry season</i>											
DOC	119	72	-27.6	-26.8	165 ± 48	-28 ± 1.2	95 ± 14.5 (-1.4, 119)	-27.3 ± 0.2	69.4 ± 46	-30.1 ± 3	77.3 ± 49
DIC	3.04	1.90	-15.0	0.53	3.8 ± 1.0	-10.6 ± 4	2.5 ± 0.3 (-0.03, 3.1)	-8.4 ± 4.8	0.9 ± 0.84	-23.5 ± 12	0.20 ± 0.3
POC	75	17.4	-27.4	-22.5	37 ± 22	-25.3 ± 2	47 ± 17 (-1.7, 75)	-26 ± 1.3	-9.5 ± 27	-26.5 ± 6	-10.5 ± 26

sources. A recent study by Suwa et al. (2020) reported above ground biomass to be $\sim 30,000 \text{ Mg km}^{-2}$ in the same mangrove location, which is much higher than the average global biomass ($11,500 \text{ Mg km}^{-2}$; Hu et al. 2020). Fine root productivity is also high ($2.7 \pm 1.9 \text{ mmol m}^{-2} \text{ h}^{-1}$; Ono et al. pers. comm., compared to Thailand mangroves: $1.4\text{--}1.7 \text{ mmol m}^{-2} \text{ h}^{-1}$; Pongpam et al. 2012). Overall, it appears that high production of biomass OC would ultimately enrich DOM concentration in the pore water and swamp surface water by active leaching of plant-derived organic acids (Cai et al. 2017).

Majority of DOC values were above the values expected from their conservative mixing, indicating the addition of DOC into the tidal creeks (or ΔC_{CMM} in Table 2, Fig. 2a). Internal recycling processes such as the production of isotopically light DOC and bacterial remineralization have been postulated as essential factors to produce such trends (Peterson et al. 1994). Furthermore, isotopic composition of DOC (-29.4‰ to -27‰) is consistent with the input from C3 plant sources (i.e., mangrove-derived DOC across a range of salinities) than C4 plants (e.g., saltmarsh, $\delta^{13}C$ usually around -12‰) or pelagic phytoplankton (around -22‰) (Gilbert et al. 2019).

Our data indicate that DOC in creek water is mostly derived from mangrove sources, leaching from pore water and swamp surface water. The DOC varied significantly with tide with higher peaks during low tide, which was seen in other studies (Dittmar and Lara 2001; Bouillon et al. 2007; Sanyal et al. 2020). Tidal variations of DOC, particularly its increase during low tide slack, may be explained by sediment–water exchange of DOC-rich pore water and its leaching into the mangrove creeks. For instance, Bouillon et al. (2007) calculated 30% of pore water-derived DOC contributing to the

surface water pool during low tide in a shallow mangrove creek in Tanzania. A clear similarity of isotopic signature of DOC in swamp water and creek water with mangrove tissues (-28.8‰ to -30.2‰ , $\delta^{13}C$ of *Avicennia* leaves: -30.5‰ ; Ray et al. 2018) supports the evidence of vegetation as the primary source of DOC particularly during low tide. Despite such similarity, we cannot rule out the possibility of DOC leaching from terrestrial plants; however, this differentiation of mangrove and terrestrial origins from the DOC pool is challenging that requires further investigation.

Particulate organic matter

The large difference of POC concentration from the watersheds to mangrove creeks (an increase of $\sim 100\%$ from watershed to creek) compared to DOC ($\sim 50\%$ increase) may be attributed to greater contribution of either mangrove-derived or algal-derived POC to the total OC pool relative to their riverine input (Table 1). Although the POC/PN atomic ratios are generally low or close to the Redfield value of 6.25 for marine algae (creek water = 7.2, swamp water = 8.4, offshore = 7.9, river water = 7.1), the high POC : Chl *a* weight ratio in the mangrove creek and swamp water ($400 \pm 152 \mu\text{g}/\mu\text{g}$) confirms the large input of detrital organic matter to the particulate organic matter (POM) pool. This is a common observation in narrow mangrove creek waters because of canopy shading that limits light penetration into the water column and subsequently limits the development of phytoplankton (e.g., Bouillon et al. 2003; Leopold et al. 2016).

As the channel widened, algal contributions progressively increased and became dominant toward the offshore where POC : Chl *a* ratios declined significantly (33–60 at $S = 33$).

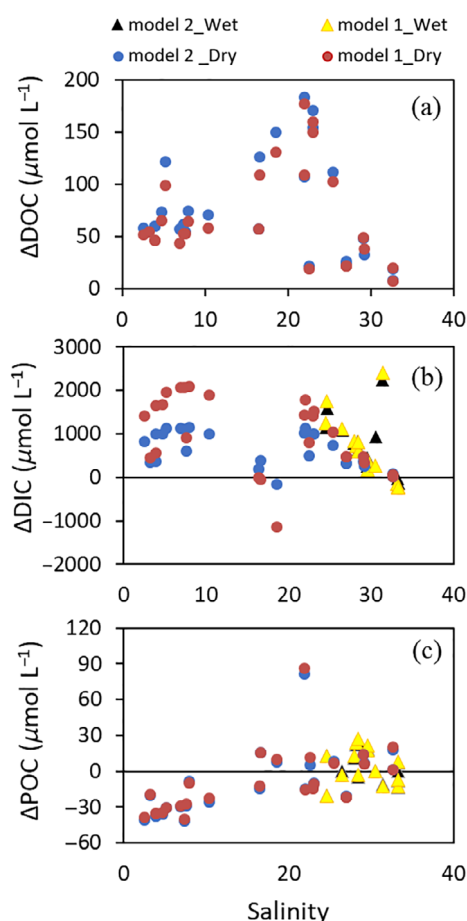


Fig. 4. Modeled concentrations within the longitudinal transect in two different seasons. Model 1 presents “internally produced” C or ΔC_{CMM} derived from Eq. 2, and Model 2 presents “mangrove-derived” C or C_{mangrove} from Eq. 5 (“Mixing model calculations to derive residual carbon” section). The ΔC_{CMM} and C_{mangrove} are labeled as ΔC in the y-axis.

The $\delta^{13}\text{C}$ values of POC were more enriched in the offshore waters (-22.7‰) indicating phytoplankton-derived carbon. An unexpected enrichment of ^{13}C in POC (-22‰) was seen in the riverine site during the wet season compared to the dry season (-27‰), which is likely a signal of microalgal sources that were visible as green patches around sampling locations at site F. Microalgae (or periphyton) sometimes show higher $\delta^{13}\text{C}$, especially when water flow rate is low like at site F (Finlay et al. 1999). Other sources such as freshwater phytoplankton or C4 plant tissues from upland and/or surrounding grasslands could also contribute to the POM pool at site F. Using an end-member value of -22‰ for algal sources and a typical value of -28‰ for C3 vegetation, it is estimated that C3 or mangrove-derived carbon contributes 44–82% to the creek water (both season), 80–90% to the river water (dry season only), 7–8% to the offshore water, 65–66% to the swamp water, and 92% to the groundwater. We noticed that intertidal sediment inside the mangrove forest with an average $\delta^{13}\text{C}$ of -26.4‰ ($n = 10$, Ray et al. unpubl. data) contains a

significant amount of C3-derived matter (84%) indicating major input from terrestrial sources. This simplified estimate of source composition of POM could be validated with additional conservative proxies such as lipid biomarkers that are used in combination with $\delta^{13}\text{C}$ (Li et al. 2020).

Tidally, high POM ratios (i.e., POC/TSS, POC/PN) and depleted $\delta^{13}\text{C}$ at low tide suggest outwelling of detritus matter during the receding tide (see POM ratios in Supporting Information Fig. S7). The peak maxima in POC/TSS % (> 10) at ebb tide indicates benthic migration and resuspension of organic-rich mangrove sediments. We observed intertidal surface sediment OC : TN ratios ranging from 18 to 24 and $\delta^{13}\text{C}$ from -26‰ to -27.5‰ (data not shown). Similar observations of POC export during receding tide are found in various mangrove settings (Tanzania, Bouillon et al. 2007; Kenya, Kitheka et al. 2002). In contrast, during the high tide, import of marine phytoplankton was evidenced by lower POM ratios and enrichment of $\delta^{13}\text{C}$ (e.g., signatures in the range -22.8‰ and -21.4‰ at $S = 23$ and 33 , respectively, Fig. 3o).

Identifying sources of DIC

The nonconservative behavior of DIC and $\delta^{13}\text{C}$ -DIC from freshwater through mangrove creeks to offshore water could result from multiple biogeochemical processes, such as OM respiration in mangrove sediment and water, air–water CO_2 exchange, carbonate dissolution, and/or groundwater discharges (Finlay 2003). The upward trend of DIC in the scatter graph (Fig. 2c) refers to DIC input at the mid-salinity zone, most likely derived from subsurface pore water leaching as a product of microbial decomposition and root respiration. This excess DIC suggests that CO_2 outgassing does not proceed as promptly as DIC production, and the actual DIC concentration would exceed DIC_{CM} due to temporary CO_2 supersaturation. Tidal control on this excess DIC is very strong especially at the beginning of low tide when a positive ΔC_{CMM} -DIC ($1170 \pm 785 \mu\text{mol L}^{-1}$), a negative $\delta^{13}\text{C}_a$ -DIC ($-18.5\text{‰} \pm 2.3\text{‰}$), and an elevated $[\text{CO}_2^*]$ in the dry season clearly confirms mangrove-derived DIC input to the creek water. Similar observations in other studies have shown concomitant increase in DIC driven by mangrove-derived organic matter respiration (Bouillon et al. 2003; Miyajima et al. 2009; Ray et al. 2020). In contrast, the relatively heavy $\delta^{13}\text{C}$ -DIC at high tide (max. -0.75‰) indicates DIC uptake by marine phytoplankton observed in both seasons ($\Delta C_{\text{CMM}} = 238 \pm 79 \mu\text{mol L}^{-1}$, $\delta^{13}\text{C}_a$ -DIC = -18.4 ± 1.3).

Carbonate chemistry and outflow of DIC from the mangroves depend largely on the corresponding alkalinity. For instance, high TA concentration in pore water and swamp waters may be attributed to sulfate reduction in the mangrove (Balk et al. 2016). An almost twofold higher pore water DIC and $[\text{CO}_2^*]$ than the overlying water suggests migration of DIC-rich slightly acidic pore waters (pH 6.9 at W5) into the water column (mean pH 7.4) at ebb flow. Sulfate reduction accounts for almost all the anaerobic diagenetic C degradation (Alongi et al. 2000) whereas iron reduction is seldom a

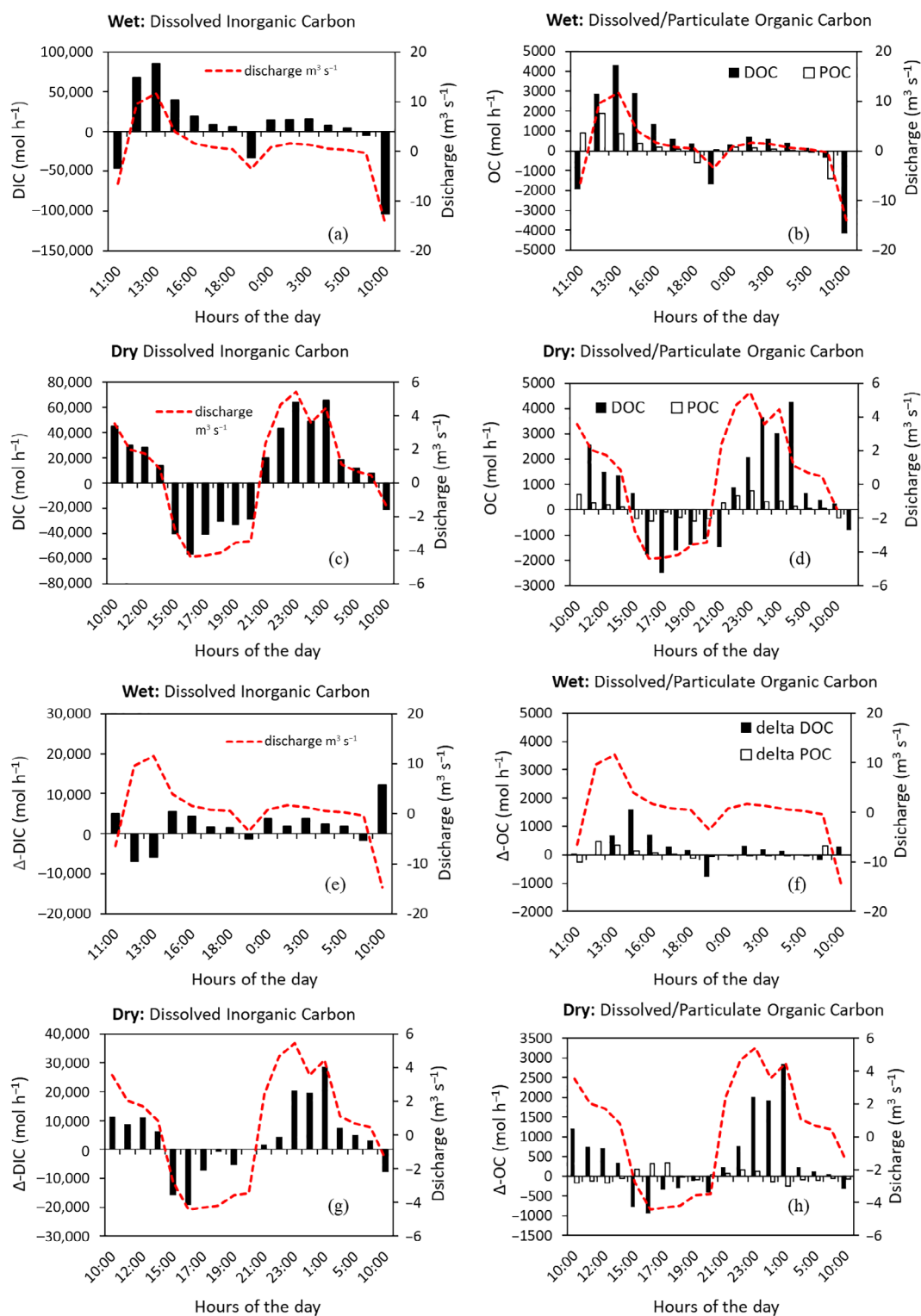


Fig. 5. Seasonal exchange fluxes (mol h^{-1}) of estuarine dissolved and particulate carbon (**a-d**) and mangrove-derived dissolved and particulate carbon (**e-h**) during time series observations in the dry and wet season.

dominant process (e.g., Thai mangrove; Kristensen and Suraswadi 2002). However, for the net alkalinity production, at least a part of sulfide produced by sulfate reduction must be

permanently sequestered somewhere avoiding reoxidation, and pyrite is one of the most likely permanent sinks of sulfide in anaerobic soils. Given the limestone-dominated feature of the

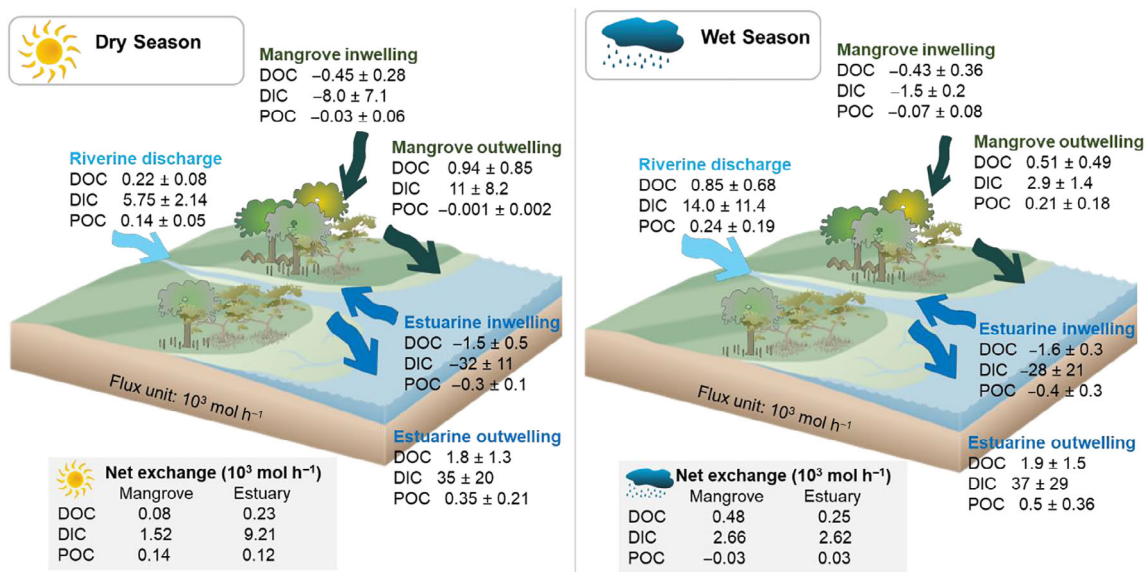


Fig. 6. Schematic presentation of carbon transport summarizing all the estimated fluxes. All units are in 10^3 mol h^{-1} to allow comparison of fluxes between different seasons and waterbodies. (symbols: Integration and Application Network, <https://ian.umces.edu/media-library/>).

KII-watershed, TA input from CaCO_3 weathering is highly plausible. Saderne et al. (2021) recognized such weathering as a potential blue carbon sink for a mangrove lying over coral rubble. Furthermore, because of low nitrate and nitrite in the creek water (median range $1.56\text{--}7.0 \mu\text{mol L}^{-1}$, data not shown), denitrification is assumed to be a minor decomposition pathway. The excess DIC at W sites and corresponding depleted $\delta^{13}\text{C}\text{-DIC}$ (Fig. 2d) could be the consequence of aerobic as well as anaerobic (mainly sulfate respiration) decomposition of soil humic substances derived from the mangroves and the isotopically lighter respiratory CO_2 delivered to the creek.

The general trend of higher ^{222}Rn concentrations upstream from the river mouth suggests greater groundwater influence from the watershed as seen in similar river-dominated mangroves (Call et al. 2018). Mean ^{222}Rn concentration in the well water is similar to that observed in other microtidal mangroves (e.g., $1539 \pm 352 \text{ Bq m}^{-3}$ from private wells in Qinglan Bay; Wu et al. 2021). Distinguishing between groundwater emitted by hydraulic pressure from aquifers located outside the ecosystem (i.e., terrestrial water), and pore water cycling within the ecosystem by tidal pumping (i.e., recirculated seawater; Stieglitz 2005) is complex and particularly important for understanding carbon dynamics in the region. In the case of terrestrial groundwater, the sources of DIC are either decomposition of terrestrial organic carbon or carbonate weathering or both. In contrast, when DIC is present in recirculated seawater, the most probable sources are decomposition of mangrove detritus and/or root respiration. For that reason, despite obtaining a significant positive relationship between carbonate parameters and ^{222}Rn (high tide vs. low tide: 35 vs. 350 Bq m^{-3} , Fig. 3r) and very high values in the pore water ($1925 \pm 832 \text{ Bq m}^{-3}$,

Table 1), it is risky to use radon as a conservative parameter in mangrove swamps and creeks. This is because radon is a noble gas and can easily escape to the atmosphere from shallow open waters in mangrove creeks. Moreover, ^{222}Rn is a radioactive isotope with a short half-life of 3.8 d, and thus rapidly lost by radioactive decay and atmospheric evasion (Cook et al. 2008). Therefore, for shallow mangrove settings, a generalization of groundwater- and pore water-derived DIC using ^{222}Rn may not be appropriate. Instead, radon results may serve only as a qualitative evidence of groundwater discharge from the watersheds outside the KII Ecopark mangroves. The high ^{222}Rn in groundwater (1290 Bq m^{-3} , Table 1) indicates groundwater discharge that may be the main source of riverine DIC in the surface water, especially during the dry season. A patchy distribution of the sediment/rock layers in the sampled area (Gabo et al. 2009) may contribute to variability in the radon-enriched groundwater.

Carbon exchange fluxes between mangroves and sea Advantages and limitations

To achieve an improved carbon flux resolution, fine-scale sampling and seasonal data collection at multiple stations are important (Dittmar and Lara 2001; Sippo et al. 2016; Ray et al. 2018). For instance, it was noticed that when ΔC decreased with increasing tidal levels, the discharge direction abruptly shifted from positive to negative (dry season, Fig. 5g,h), which means that a slight change in ΔC could change the daily flux estimation drastically. But such fluctuation can be minimized by short-interval water sampling (e.g., 30 min, in this study). Furthermore, flux error can be significant owing to system heterogeneity, for example, presence of nonmangroves species, fluctuation in elevation, and creek size. For

example, 25% error in carbon flux was reported for large creeks (Call et al. 2019). As the KII Ecopark creeks are relatively narrow, the watershed is small, and the forest has high cover of true mangrove species and associates, flux error owing to heterogeneity should be less significant. Furthermore, 88% of the KII Ecopark mangrove floor remain inundated during high tide (i.e., 0.39 km², from digital elevation modeling result) meaning that when the water level decreases, the majority of mangrove materials are likely to be flushed out to the sea, favored by the gentle slope of the creeks, a condition ideal for detecting carbon outwelling (Adame and Lovelock 2011).

Uncertainty in carbon flux estimate in estuaries is sensitive to the method used, with some methods resulting in very large uncertainties. This study follows the most common Lagrangian method that integrates water discharge volume and element concentrations over different time periods which is used for the delineated catchments (Twilley and Rivera-Monroy 2009). Unlike most of the previous flux estimates, we have considered internally produced or mangrove-derived carbon (ΔC , Eq. 2) rather than the absolute concentrations to determine fate of the “actual amount of carbon” delivered from the mangrove waters (similar to works by Ho et al. 2017; Ray et al. 2018, 2020; Ohtsuka et al. 2020; Reithmaier et al. 2020). Likewise, stable isotope mixing models should be critically evaluated. While short-lived radioisotope (like radium) may provide accurate carbon flux estimate for the fringing shoreline (Sippo et al. 2019), stable isotope ratios of carbon are more applicable to riverine types with distinct salinity gradient like the KII Ecopark. The assumption of POC being conservatively mixed should be restricted to the relatively clear water such as KII Ecopark with TSS < 5 mg L⁻¹ at $S = 33$ given the importance of deposition, resuspension, and the existence of mobile mud bed (e.g., French Guiana with TSS > 170 mg L⁻¹ at $S = 35$; Ray et al. 2018).

The major limitations of the present flux estimates are summarized in Supporting Information Table S3. Although their effects on the present flux estimates are unknown, qualitative assessment of the influence of a wide range of processes including hydrological, ecological, and water-atmosphere exchange remain important. For example, due to the high level of connectivity between the watershed and creeks (Fig. 1), the creek that is connected to the river upstream is assumed to deliver more “green” carbon to the river mouth than the disconnected creek that might bring more “blue” carbon (i.e., mangrove-derived). While multiple site observations done frequently at W5 (without river-end) and occasionally at W4 (with river-end) comprised the organic fractions of both “green” and “blue” carbon delivered to the sea and deposited in sediment, a successful assessment of the provenance and fate of blue carbon could be obtained by applying more advanced tools such as molecular biomarkers and environmental DNA in the depositional region (Geraldi et al. 2019).

Seasonal carbon exchange fluxes

In contrast to estuarine and mangrove-derived fluxes, riverine carbon export differs considerably between seasons mainly because of the changing rainfall pattern rather than river discharges (see limitation in Supporting Information Table S3). However, seasonal differences appear to have little influence on the estuarine and mangrove-derived carbon fluxes due to the relatively uniform carbon concentrations and water exchange rates throughout the sampling periods (see data of C_{obs} , ΔC_{CMM} , and $C_{mangrove}$, Table 2). An exception was POC since both estuarine and mangrove-derived POC fluxes were significantly higher in the wet season than the dry season. In contrast to dissolved carbon forms, POC appears to be influenced more by seasonal variations in productivity/litter input (Adame and Lovelock 2011), and cumulative impact of water current velocities and river runoff that induce greater export of POC in mangrove systems (Romigh et al. 2006). At the KII Ecopark, these hydrological factors were dominant during the wet season observations (water current and run off: dry $0.05 \pm 0.03 \text{ m s}^{-1}$ and $0.53 \pm 0.19 \text{ m}^3 \text{ s}^{-1}$, wet $0.17 \pm 0.10 \text{ m s}^{-1}$ and $0.98 \pm 0.79 \text{ m}^3 \text{ s}^{-1}$, respectively). The entire river estuary acts as net exporter of carbon, with the dissolved forms dominating the total export flux. In the case of exported OC, DOC remains the major form with DOC : POC of 3.2 ± 0.75 , which is higher than the ratios observed globally in mangrove waters (> 1.5; Bouillon et al. 2007). In addition, high water discharge due to seasonal typhoons could enhance organic carbon export from mangrove forest (Ohtsuka et al. 2020) such was observed in Panay Island where reduction of 40–50% organic matter in eroded mangrove soil was reported after successive severe typhoons in the past (Salmo 2021).

Although export flux of DIC from mangroves have been very rarely estimated until recently (12 estimates in the last 8 years, updated from the review by Alongi 2020), it is now widely accepted that mangrove estuaries tend to show higher DIC export than DOC and POC. This is because DIC concentrations are commonly high, and the water column is supersaturated with CO₂ (Borges et al. 2003). This is consistent with our findings where DIC : OC exceeds 300, and DIC contributes 92–94% to total carbon input from the river, 84–90% to mangrove-derived export, and 91–96% to estuarine export (taking both season into account, Fig. 6). Similar empirical data are reported for the world’s largest Sundarbans mangrove where DIC contributed 91% to the total riverine input, and DOC and DIC together contributed 92% to the mangrove-C export to the Bay of Bengal (Ray et al. 2018). Ho et al. (2017) found DIC contributed 82–83% to the dissolved carbon fluxes at the Shark River, Everglades Florida. According to Wu et al. (2021), DIC contributed 98% to the total mangrove groundwater-derived dissolved carbon export in Hainan Bay. Since DIC and TA are highly correlated in KII mangroves ($r^2 = 0.99$), the riverine and mangrove-derived TA may also be a significant source of alkalinity to the Sibuyan Sea. The TA input from the mangroves may partially

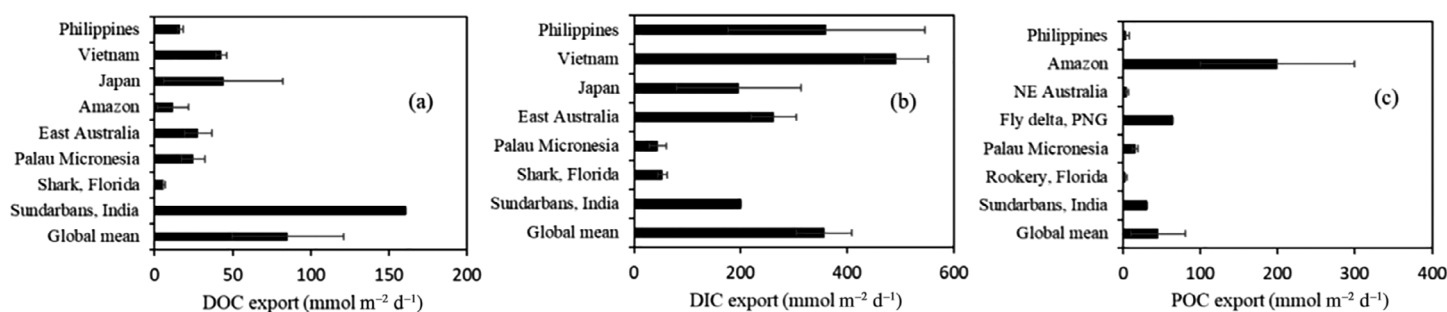


Fig. 7. Comparison of carbon export/import fluxes as DOC, POC, and DIC between this study and selected mangroves around the world (unit: $\text{mmol m}^{-2} \text{d}^{-1}$). Uncertainties in mean fluxes are linked to seasonal variability in our study site. Data source: Amazon and Brazil: Dittmar and Lara (2001), Dittmar et al. (2006); Florida: Romigh et al. (2006), Ho et al. (2017); Micronesia: Call et al. (2019); India: Ray et al. (2018); East Australia: Maher et al. (2013); NE Australia: Sippo et al. (2016); Fly delta, PNG: Robertson and Alongi (1995); Vietnam: Taillardat et al. (2018); Japan: Ohtsuka et al. (2020); Global mean: Alongi (2020).

provide a localized buffering effect against coastal acidification as reported for the Australian mangroves (Sippo et al. 2016).

Mangrove contribution to carbon outwelling

Mangrove-derived outwelling fluxes of DOC and DIC contribute 27–53% and 8–31% to estuarine outwelling fluxes, respectively (Fig. 6). These estimates are expected since mangroves are key sources of internally produced DOC (mangrove leaching) and DIC (sulfate reduction plus aerobic respiration), with the latter having external sources as well (carbonate weathering in the watershed). However, 8–31% of DIC flux attributed to mangroves is low compared to other estimates (Fig. 7). This is probably because of the microtidal nature of the estuary where there is less tidal pumping and advection compared to mangroves subjected to a larger tidal prism. In the case of POC, 42% of the estuarine flux is contributed by the mangroves in the wet season owing to rapid movement of floating detritus carried by strong seasonal water currents. In the dry season, negative POC flux or inwelling in the mangrove zone indicates retention of OC in the suspended matter probably due to low rainfall and river discharge that hinder transport of POC (e.g., Iriomote Island, Akhand et al. 2021; French Guiana, Ray et al. 2020). Therefore, import and export fluxes of POC of different origins may be closely balanced (e.g., Ayukai et al. 1998), leaving only a small residual net flux from the KII creek water to the Sibuyan Sea. Overall, the riverine (inbound to creek) and net mangrove plus estuarine carbon (outbound to sea) export produce an unresolved flux that was higher in the wet season (dry: 5.2 ± 2.8 , wet: $9.1 \pm 4.3 \times 10^3 \text{ mol h}^{-1}$) probably attributable to DIC removal processes during its passage to the sea (mainly as CO_2 outgassing is shown by higher $[\text{CO}_2^*]$ during high flow conditions, Table 1, Fig. 3i,j).

Globally, carbon flux data in mangrove estuaries are limited. The reports available differ from one another because of the different biogeographic setting and hydrological conditions. However, this study shows that area-weighted fluxes of DOC and POC for our study site are well within the ranges of

other regional estimates except for DIC that is notably higher in the Philippines (Fig. 7). Nevertheless, comparisons of flux data among different hydrogeographic regions should consider the potential of methodological bias where different methods to obtain flux estimates have been used for the mangrove-dominated coastal and estuarine system.

Conclusion

The present study examined the spatiotemporal variability and exchange fluxes of DOC, DIC, and POC in a riverine mangrove system in Panay Island (Philippines) by following a robust sampling strategy. Carbon exchange fluxes were estimated using high resolution (30 min) surface and bottom water sampling from multiple points covering both dry and wet seasons and tidal range variation (full spring and transient neap). We found that mangroves are potential exporters of DOC and DIC in intertidal waters, while lithogenic sources control the watershed carbonate chemistry. Riverine, mangrove and estuarine fluxes reveal significant outwelling of blue carbon into the Sibuyan Sea. With these first baseline carbon flux estimates from a microtidal mangrove in the Philippines, it can be concluded that a significant fraction of mangrove-derived carbon is delivered from the mangrove to the sea, and that global carbon outwelling estimates from mangroves differ because of differences in methodologies and hydroclimatic settings.

References

- Adame, M. E., and C. E. Lovelock. 2011. Carbon and nutrient exchange of mangrove forests with the coastal ocean. *Hydrobiologia* **663**: 23–50. doi:10.1007/s10750-010-0554-7
- Akhand, A., and others. 2021. Lateral carbon fluxes and CO_2 evasion from a subtropical mangrove-seagrass-coral continuum. *Sci. Total Environ.* **752**: 142190. doi:10.1016/j.scitotenv.2020.142190
- Alling, V., D. Porcelli, C. M. Morth, L. G. Anderson, L. Sanchez-Garcia, O. Gustafsson, P. S. Andersson, and C. Humborg. 2012. Degradation of terrestrial organic carbon,

- primary production and out-gassing of CO₂ in the Laptev and East Siberian Seas as inferred from δ¹³C values of DIC. *Geochim. Cosmochim. Acta* **95**: 143–159. doi:10.1016/j.gca.2012.07.028
- Alongi, D. M. 2020. Carbon cycling in the world's mangrove ecosystems revisited: Significance of non-steady state diagenesis and subsurface linkages between the forest floor and the coastal ocean. *Forests* **11**: 977. doi:10.3390/f11090977
- Alongi, D. M., E. Tirendi, and B. F. Clough. 2000. Below-ground decomposition of organic matter in forests of the mangroves *Rhizophora stylosa* and *Avicennia marina* along the arid coast of Western Australia. *Aquat. Bot.* **68**: 97–122. doi:10.1016/S0304-3770(00)00110-8
- Ayukai, T., D. Miller, E. Wolanski, and S. Spagnol. 1998. Fluxes of nutrients and dissolved and particulate organic carbon in two mangrove creeks in northeastern Australia. *Mangroves Salt Marshes* **2**: 223–230. doi:10.1023/A:1009923410116
- Balk, M., J. A. Keuskamp, and H. J. Laanbroek. 2016. Potential for sulfate reduction in mangrove forest soils: Comparison between two dominant species of the Americas. *Front. Microbiol.* **7**: 1855. doi:10.3389/fmicb.2016.01855
- Barrientos, K. D., and J. W. Apolonio. 2017. Species diversity and soil carbon sequestration potential of mangrove species at Katunggan It Ibajay (KII) Eco-Park in Aklan, Philippines. *PRISM, The Official Research Publication of Negros Oriental State University* **22**: 1–13. <https://ssrn.com/abstract=3824652>
- Blanco, A. C., A. Watanabe, K. Nadaoka, S. Motooka, E. C. Herrera, and T. Yamamoto. 2011. Estimation of nearshore groundwater discharge and its potential effects on a fringing coral reef. *Mar. Pollut. Bull.* **62**: 770–785. doi:10.1016/j.marpolbul.2011.01.005
- Borges, A. V., S. Djenidi, G. Lacroix, J. Theate, B. Delille, and M. Frankignoulle. 2003. Atmospheric CO₂ flux from mangrove surrounding waters. *Geophys. Res. Lett.* **30**: 1558. doi:10.1029/2003GL017143
- Bouillon, S., M. Frankignoulle, F. Dehairs, B. Velimirov, A. Eiler, H. Etcheber, G. Abril, and A. V. Borges. 2003. Inorganic and organic carbon biogeochemistry in the Gautami Godavari estuary (Andhra Pradesh, India) during pre-monsoon: The local impact of extensive mangrove forests. *Global Biogeochem. Cycl.* **17**. doi:10.1029/2002GB00202
- Bouillon, S., J. J. Middelburg, F. Dehairs, A. V. Borges, G. Abril, M. R. Flindt, S. Ulomi, and E. Kristensen. 2007. Importance of intertidal sediment processes and porewater exchange on the water column biogeochemistry in a pristine mangrove creek (Ras Dege, Tanzania). *Biogeosciences* **4**: 311–322. doi:10.5194/bg-4-311-2007
- Cai, D., X. Yang, S. Wang, Y. Chao, J. L. Morel, and R. Qiu. 2017. Effects of dissolved organic matter derived from forest leaf litter on biodegradation of phenanthrene in aqueous phase. *J. Hazard. Mater.* **324**: 516–525. doi:10.1016/j.jhazmat.2016.11.020
- Call, M., C. J. Sanders, A. Enrich-Prast, L. Sanders, H. Marotta, I. R. Santos, and D. T. Maher. 2018. Radon-traced pore-water as a potential source of CO₂ and CH₄ to receding black and clear water environments in the Amazon Basin. *Limnol. Oceanogr. Lett.* **3**: 375–383. doi:10.1002/lo2.10089
- Call, M., C. J. Sanders, P. A. Macklin, I. R. Santos, and D. T. Maher. 2019. Carbon outwelling and emissions from two contrasting mangrove creeks during the monsoon storm season in Palau, Micronesia. *Estuar. Coast. Shelf Sci.* **218**: 340–348. doi:10.1016/j.ecss.2019.01.002
- Carpenter, I. H., W. L. Bradford, and V. Grant. 1975. Processes affecting the composition of estuarine waters, p. 188–214. *In* L. E. Cronin [ed.], *Estuarine research V.1*. Academic.
- Chen, X., Y. Lao, J. Wang, J. Du, M. Liang, and B. Yang. 2018. Submarine groundwater-borne nutrients in a tropical bay (Maowei Sea, China) and their impacts on the oyster aquaculture. *Geochem. Geophys. Geosyst.* **19**: 932–951. doi:10.1002/2017GC007330
- Cook, P. G., C. Wood, T. White, C. T. Simmons, T. Fass, and P. Brunner. 2008. Groundwater inflow to a shallow, poorly-mixed wetland estimated from a mass balance of radon. *J. Hydrol.* **354**: 213–226. doi:10.1016/j.jhydrol.2008.03.016
- Dittmar, T., and R. J. Lara. 2001. Do mangroves rather than rivers provide nutrients to coastal environments south of the Amazon River? Evidence from long-term flux measurements. *Mar. Ecol. Prog. Ser.* **213**: 67–77.
- Dittmar, T., N. Hertkorn, G. Kattner, and R. J. Lara. 2006. Mangroves, a major source of dissolved organic carbon to the oceans. *Global Biogeochem. Cycl.* **20**(1): 1–7. doi:10.1029/2005GB002570
- Donato, D. C., J. B. Kauffman, D. Murdiyarsa, S. Kurnianto, M. Stidham, and M. Kanninen. 2011. Mangroves among the most carbon-rich forests in the tropics. *Nat. Geosci.* **4**: 293–297. doi:10.1038/ngeo1123
- Duarte, C. M., J. Middelburg, and N. Caraco. 2005. Major role of marine vegetation on the oceanic carbon cycle. *Biogeosciences* **1**: 1–8. doi:10.5194/bg-2-1-2005
- Finlay, J. C. 2003. Controls of streamwater dissolved inorganic carbon dynamics in a forested watershed. *Biogeochemistry* **62**: 231–252.
- Finlay, J. C., M. E. Power, and G. Cabana. 1999. Effects of water velocity on algal carbon isotope ratios: Implications for river food web studies. *Limnol. Oceanogr.* **44**: 1198–1210. doi:10.4319/lo.1999.44.5.1198
- Fourqurean, J. W., and others. 2012. Seagrass ecosystems as a globally significant carbon stock. *Nat. Geosci.* **5**: 505–509. doi:10.1038/ngeo1477
- Gabo, J. A. S., C. B. Dimalanta, M. G. S. Asio, K. L. Queaño, G. P. Yumul, and A. Imai. 2009. Geology and geochemistry of the clastic sequences from Northwestern Panay (Philippines): Implications for provenance and geotectonic

- setting. *Tectonophysics* **479**: 111–119. doi:[10.1016/j.tecto.2009.02.004](https://doi.org/10.1016/j.tecto.2009.02.004)
- Geraldi, N. R., and others. 2019. Fingerprinting blue carbon: Rationale and tools to determine the source of organic carbon in marine depositional environments. *Front. Mar. Sci.* **6**: 263. doi:[10.3389/fmars.2019.00263](https://doi.org/10.3389/fmars.2019.00263)
- Gilbert, P. M., J. J. Middelburg, J. W. McClelland, and J. V. Zanden. 2019. Stable isotope tracers: Enriching our perspectives and questions on sources, fates, rates, and pathways of major elements in aquatic systems. *Limnol. Oceanogr.* **64**: 950–981. doi:[10.1002/lno.11087](https://doi.org/10.1002/lno.11087)
- Giri, C., E. Ochieng, L. L. Tieszen, Z. Zhu, A. Singh, T. Loveland, J. Masek, and N. Duke. 2011. Status and distribution of mangrove forests of the world using earth observation satellite data. *Glob. Ecol. Biogeogr.* **20**: 154–159. doi:[10.1111/j.1466-8238.2010.00584.x](https://doi.org/10.1111/j.1466-8238.2010.00584.x)
- González, J., N. Tejedor-Flores, and R. Pinzón. 2019. A bibliographic review of the importance of carbon dioxide capture in mangroves, p. 126–131. *In* 7th International Engineering, Sciences and Technology Conference (IESTEC), Panama, Panama, v. **2019**. doi:[10.1109/IESTEC46403.2019.00-89](https://doi.org/10.1109/IESTEC46403.2019.00-89)
- Ho, D. T., S. Ferrón, V. C. Engel, W. T. Anderson, P. K. Swart, R. M. Price, and L. Barbero. 2017. Dissolved carbon biogeochemistry and export in mangrove dominated rivers of the Florida Everglades. *Biogeosciences* **14**: 2543–2559. doi:[10.5194/bg-14-2543-2017](https://doi.org/10.5194/bg-14-2543-2017)
- Howard, J., A. Sutton-Grier, D. Herr, J. Kleypas, E. Landis, E. Mcleod, E. Pidgeon, and S. Simpson. 2017. Clarifying the role of coastal and marine systems in climate mitigation. *Front. Ecol. Environ.* **15**: 42–50.
- Hu, T., Y. Y. Zhang, Y. Su, Y. Zheng, G. Lin, and Q. Guo. 2020. Mapping the global mangrove Forest aboveground biomass using multisource remote sensing data. *Remote Sens.* **12**: 1690. doi:[10.3390/rs12101690](https://doi.org/10.3390/rs12101690)
- Kitheka, J. U., G. S. Ongwenyi, and K. M. Mavuti. 2002. Dynamics of suspended sediment exchange and transport in a degraded mangrove creek in Kenya. *Ambio* **31**: 580–587.
- Kobayashi, S., and others. 2015. The JRA-55 reanalysis: General specifications and basic characteristics. *J. Met. Soc. Jpn.* **93**: 5–48. doi:[10.2151/jmsj.2015-001](https://doi.org/10.2151/jmsj.2015-001)
- Krause-Jensen, D., and C. M. Duarte. 2016. Substantial role of macroalgae in marine carbon sequestration. *Nat. Geosci.* **9**: 737–742. doi:[10.1038/ngeo2790](https://doi.org/10.1038/ngeo2790)
- Kristensen, E., and P. Suraswadi. 2002. Carbon, nitrogen and phosphorus dynamics in creek water of a Southeast Asian mangrove forest. *Hydrobiologia* **474**: 197–211. doi:[10.1023/A:1016544006720](https://doi.org/10.1023/A:1016544006720)
- Kristensen, E., R. M. Connolly, X. L. Otero, C. Marchand, T. O. Ferreira, and V. H. Rivera-Monroy. 2017. Biogeochemical cycles: Global approaches and perspectives, p. 163–209. *In* V. H. Rivera-Monroy, S. Y. Lee, E. Kristensen, and R. R. Twilley [eds.], *Mangrove ecosystems: A global and biogeographic perspectives*. Springer. doi:[10.1007/978-3-319-62206-4_6](https://doi.org/10.1007/978-3-319-62206-4_6)
- Kurihara, H., and others. 2021. Potential local adaptation of corals at acidified and warmed Nikko Bay, Palau. *Sci. Rep.* **11**: 1–10. doi:[10.1038/s41598-021-90614-8](https://doi.org/10.1038/s41598-021-90614-8)
- Lebata, M. J. H. L. 2006. Stock enhancement of the mud crabs *Scylla* spp. in the mangroves of Naisud and Bugtong Bato, Ibaday, Aklan, Philippines. Ph.D. dissertation, Univ. of Wales.
- Lee, S. Y. 1995. Mangrove outwelling: A review. *Hydrobiologia* **295**: 203–212. doi:[10.1007/BF00029127](https://doi.org/10.1007/BF00029127)
- Leopold, A., C. Marchand, J. Deborde, and M. Allenbach. 2016. Water biogeochemistry of a mangrove-dominated estuary under a semi-arid climate (New Caledonia). *Estuar. Coast.* **40**: 773–791. doi:[10.1007/s12237-016-0179-9](https://doi.org/10.1007/s12237-016-0179-9)
- Lewis, E., and D. W. R. Wallace. 1998. Program developed for CO₂ system calculations. Carbon Dioxide Information Analysis Center, Oak Ridge National Laborator.
- Li, Z., Y. Sun, and X. Nie. 2020. Biomarkers as a soil organic carbon tracer of sediment: Recent advances and challenges. *Earth Sci. Rev.* **208**: 103277. doi:[10.1016/j.earscirev.2020.103277](https://doi.org/10.1016/j.earscirev.2020.103277)
- Maher, D. T., I. R. Santos, L. Golsby-Smith, J. Gleeson, and B. D. Eyre. 2013. Groundwater-derived dissolved inorganic and organic carbon exports from a mangrove tidal creek: The missing mangrove carbon sink? *Limnol. Oceanogr.* **58**: 475–488. doi:[10.4319/lo.2013.58.2.0475](https://doi.org/10.4319/lo.2013.58.2.0475)
- Maher, D. T., M. Call, I. R. Santos, and C. J. Sanders. 2018. Beyond burial: Lateral exchange is a significant atmospheric carbon sink in mangrove forests. *Biol. Lett.* **14**: 20180200. doi:[10.1098/rsbl.2018.0200](https://doi.org/10.1098/rsbl.2018.0200)
- Miyajima, T., Y. Tsuboi, Y. Tanaka, and I. Koike. 2009. Export of inorganic carbon from two Southeast Asian mangrove forests to adjacent estuaries as estimated by the stable isotope composition of dissolved inorganic carbon. *J. Geophys. Res.* **114**: G01024. doi:[10.1029/2008JG000861](https://doi.org/10.1029/2008JG000861)
- Mook, W. G., and T. C. Tan. 1991. Stable carbon isotopes in rivers and estuaries, p. 245–264. *In* E. T. Degens, S. Kempe, and J. E. Richey [eds.], *Biogeochemistry of major world rivers*. John Wiley and Sons, Ltd.
- Odum, E. P. 1968. Energy flow in ecosystems: A historical review. *Am. Zool.* **8**: 11–18.
- Ohtsuka, T., and others. 2020. Lateral export of dissolved inorganic and organic carbon from a small mangrove estuary with tidal fluctuation. *Forests* **11**: 1041. doi:[10.3390/f11101041](https://doi.org/10.3390/f11101041)
- Peterson, B., B. Fry, M. Hullar, S. Saube, and R. Wright. 1994. The distribution and stable carbon isotopic composition of dissolved organic carbon in estuaries. *Estuaries* **17**: 111–121. doi:[10.2307/1352560](https://doi.org/10.2307/1352560)
- Poungparn, S., A. Komiyama, T. Sangteian, C. Maknual, P. Patanaponpaiboon, and V. Suchewaboripont. 2012. High primary productivity under submerged soil raises the net

- ecosystem productivity of a secondary mangrove forest in eastern Thailand. *J. Trop. Ecol.* **28**: 303–306.
- Primavera, J.H., R.S. Sadaba, M.J.H.L. Leбата and J.R Altamirano. 2004. Handbook of Mangroves in the Philippines – Panay. SEAFDEC Aquaculture Department, Iloilo, Philippines. 106 pp.
- Ray, R., A. Baum, G. Gleixner, T. Rixen, and T. K. Jana. 2018. Exportation of dissolved (inorganic and organic) and particulate carbon from mangroves and their implications to the carbon budget in the Indian Sundarbans. *Sci. Total Environ.* **621**: 535–547. doi:10.1016/j.scitotenv.2017.11.225
- Ray, R., and others. 2018. Sources and distribution of carbon (DOC, POC, DIC) in a mangrove dominated estuary (French Guiana, South America). *Biogeochemistry* **138**: 297–321. doi:10.1007/s10533-018-0447-9
- Ray, R., G. Thouzeau, R. Walcker, V. Vantrepotte, S. Morvan, J. Devesa, M. le Goff, and E. Michaud. 2020. Mangrove-derived organic and inorganic carbon export to the Atlantic Ocean? Time series study in the Guianese estuarine system, Latin America. *J. Geophys. Res. Biogeosci.* **125**: e2020JG005739. doi:10.1029/2020JG005739
- Reithmaier, G. M. S., D. Ho, S. G. Johnston, and D. T. Maher. 2020. Mangroves as a source of greenhouse gases to the atmosphere and alkalinity and dissolved carbon to the Coastal Ocean: A case study from the Everglades National Park, Florida. *J. Geophys. Res. Biogeosci.* **125**: 22020JG005812. doi:10.1029/2020JG005812
- Robertson, A. I., and D. M. Alongi. 1995. Role of riverine mangrove forest in organic carbon export to the tropical coastal ocean: A preliminary mass balance for the Fly Delta (Papua New Guinea). *Geo-Mar. Lett.* **15**: 134–139. doi:10.1007/BF01204454
- Romigh, M. A., S. E. David, V. H. Rivera-Monroy, and R. R. Twilley. 2006. Flux of organic carbon in a riverine mangrove wetland in the Florida Coastal Everglades. *Hydrobiologia* **569**: 505–516. doi:10.1007/s10750-006-0152-x
- Saderne, V., M. Fusi, T. Thomson, A. Dunne, F. Mahmud, F. Roth, S. Carvalho, and C. M. Duarte. 2021. Total alkalinity production in a mangrove ecosystem reveals an overlooked Blue Carbon component. *Limnol. Oceanograph. Lett.* **6**: 61–67. doi:10.1002/lo12.10170
- Salmo, III S.G., 2021. Assessment of typhoon impacts and post-typhoon recovery in Philippine mangroves: lessons and challenges for adaptive management. Chapter 21, in book : Dynamic Sedimentary Environments of Mangrove Coasts. Ed. Frida Sidik & Dan Friess pp540–559, 367. Imprint Elsevier ISBN 9780128164372.
- Sánchez-Carrillo, S., R. Sánchez-Andrés, L. C. Alatorre, D. G. Angeler, M. Álvarez-Cobelas, and J. A. Arreola-Lizárraga. 2009. Nutrient fluxes in a semi-arid microtidal mangrove wetland in the Gulf of California. *Estuar. Coast. Shelf Sci.* **82**: 654–662.
- Santos, I. R., and others. 2021. The renaissance of Odum's outwelling hypothesis in “Blue Carbon” science. *Estuar. Coast. Shelf Sci.* **255**: 107361. doi:10.1016/j.ecss.2021.107361
- Sanyal, P., R. Ray, M. Paul, V. K. Gupta, A. Acharya, S. Bakshi, T. K. Jana, and S. K. Mukhopadhyay. 2020. Assessing the dynamics of dissolved organic matter (DOM) in the coastal environments dominated by mangroves. *Indian Sundarbans. Front. Earth Sci.* **8**: 218. doi:10.3389/feart.2020.00218
- Sato, T., T. Miyajima, H. Ogawa, Y. Umezawa, and I. Koike. 2006. Temporal variability of stable carbon and nitrogen isotopic composition of size-fractionated particulate organic matter in the hypertrophic Sumida River Estuary of Tokyo Bay. Japan. *Estuar. Coast. Shelf Sci.* **68**: 245–258. doi:10.1016/j.ecss.2006.02.007
- Scheibe, A., L. Krantz, and G. Gleixner. 2012. Simultaneous determination of the quantity and isotopic signature of dissolved organic matter from soil water using high-performance liquid chromatography/isotope ratio mass spectrometry. *Rapid Commun. Mass Spectrom.* **26**: 173–180. doi:10.1002/rcm.5311
- Sippo, J. Z., D. T. Maher, D. R. Tait, C. Holloway, and I. R. Santos. 2016. Are mangroves drivers or buffers of coastal acidification? Insights from alkalinity and dissolved inorganic carbon export estimates across a latitudinal transect. *Global Biogeochem. Cycl.* **30**: 753–766. doi:10.1002/2015GB005324
- Sippo, J. Z., D. T. Maher, K. G. Schulz, C. J. Sanders, A. McMahon, J. Tucker, and I. R. Santos. 2019. Carbon outwelling across the shelf following a massive mangrove dieback in Australia: Insights from radium isotopes. *Geochim. Cosmochim. Acta* **253**: 142–158. doi:10.1016/j.gca.2019.03.003
- Stieglitz, T. 2005. Submarine groundwater discharge into the near-shore zone of the Great Barrier Reef, Australia. *Mar. Pollut. Bull.* **51**: 51–59. doi:10.1016/j.marpolbul.2004.10.055
- Suwa, R., and others. 2020. Mangrove biomass estimation using canopy height and wood density in the South East and East Asian regions. *Estuar. Coast. Shelf Sci.* **248**: 106937. doi:10.1016/j.ecss.2020.106937
- Taillardat, P., and others. 2018. Assessing the contribution of porewater discharge in carbon export and CO₂ evasion in a mangrove tidal creek (Can Gio, Vietnam). *J. Hydrol.* **563**: 303–318. doi:10.1016/j.jhydrol.2018.05.042
- Tan, M. L., P. W. Gassman, R. Srinivasan, J. G. Arnold, and X. Yang. 2019. A review of SWAT studies in Southeast Asia: Applications, challenges and future directions. *Water* **11**: 914. doi:10.3390/w11050914
- Twilley, R. R., and V. H. Rivera-Monroy. 2009. Ecogeomorphic models of nutrient biogeochemistry for mangrove wetlands, p. 641–683. *In* G. M. E. Perillo, E. Wolanski, D. R. Cahoon, and M. M. Brinson [eds.], *Coastal wetlands: An integrated ecosystem approach*. Elsevier.
- U.S. Office of Surface Mining Reclamation and Enforcement 2012. Well purging procedures for obtaining valid water

- samples from domestic and monitoring wells [accessed 2012 May 05]. p. 2. Available from www.arcc.osmre.gov
- Ward, N. D., and others. 2020. Representing the function and sensitivity of coastal interfaces in Earth system models. *Nat. Commun.* **11**: 2458. doi:[10.1038/s41467-020-16236-2](https://doi.org/10.1038/s41467-020-16236-2)
- Watanabe, K., Yoshida, G., Hori, M., Umezawa, Y., Moki, H., and Kuwae, T. 2020. Macroalgal metabolism and lateral carbon flows can create significant carbon sinks. *Biogeosci.* **17**: 2425-2440.
- Wickham, H., R. François, L. Henry, and K. Müller. 2020. *dplyr: A grammar of data manipulation*. R package version 1.0.2. Available from <https://CRAN.R-project.org/package=dplyr>
- Wu, Z., H. Zhu, D. Tang, Y. Wang, A. Zidan, and Z. Cui. 2021. Submarine groundwater discharge as a significant export of dissolved inorganic carbon from a mangrove tidal creek to Qinglan Bay (Hainan Island, China). *Cont. Shelf Res.* **223**: 104451. doi:[10.1016/j.csr.2021.104451](https://doi.org/10.1016/j.csr.2021.104451)
- (SATREPS) for financially supporting the Project “Comprehensive Assessment and Conservation of Blue Carbon Ecosystems and their Services in the Coral Triangle (BlueCARES).” We are indebted to Dr Gerd Gleixner and Steffen Ruehlow (MPI-Jena, Germany) for providing support in $\delta^{13}\text{C}$ analyses, and Dr Naoko Morimoto for POM analyses. We sincerely thank Dr Kenji Ono for sharing fine root production data. We are thankful to Dr Ariel Blanco (Department of Geodetic Engineering, UP Diliman) for providing delineation of mangrove area and Dr. Enrico C. Paringit, program leader of Phil-LiDAR 1, for providing the LiDAR products for map preparation. We thank Jeffrey Munar, Jesus Abad, John Michael Aguilar, Dominic Bautista, Bryan C. Hernandez and Mr Tsuyoshi Kanda for their assistance during field surveys. We are grateful for the overall support given by the University of the Philippines, Diliman and Aklan State University to the project. Finally, we thank the Journal Editor, Associate Editor, and three reviewers for their valuable comments and corrections on the manuscript.

Conflict of interest

None declared.

Acknowledgments

We are grateful to the Japan International Cooperation Agency (JICA) and Japan Science and Technology Agency (JST) through the Science and Technology Research Partnership for Sustainable Development Program

Submitted 03 February 2021

Revised 01 July 2021

Accepted 01 September 2021

Associate editor: Catherine Ellen Lovelock